# Optimal Control Adjoint Method for Inversion in Wave Propagation

Eftychia V. Karasmani

graduated from the Department of Applied Mathematics of the University of Crete

*Supervisor:* John S. Papadakis

*Readers:* John S. Papadakis, Michael I. Taroudakis,
George N. Makrakis

Submitted in partial fulfilment of the requirements for the degree of

Master of Science in *Optics and Vision*

of the Departments of Medicine, Mathematics, Physics,

Materials Science and Technology,

at University of Crete, in Heraklion

March 17, 2010

## Abstract

We suppose that the wave propagation inside a medium is modelled by a well posed mathematical problem. Specifically, the adopted model consists of:

1. the properties of the medium (e.g., density, wave speed, attenuation, etc.)
2. the properties and the location of the source
3. the boundary conditions
4. the propagated field.

We choose to write the above problem in terms of a system of partial differential equations with initial and boundary conditions.

The task of specifying the propagated field when the properties of the medium, the properties and the location of the source as well as the boundary conditions are assumed to be known, is called the **Direct Problem**. We suppose that we can obtain a numerical solution for this problem, using an appropriate model.

On the other hand, an **Inverse Problem** arise when the propagated field is assumed to be known by experimental measurements and the objective is to recover the properties of the medium, or find the location and the properties of the source, or even determine the boundary conditions. A solution for the Inverse problem can be derived by minimizing the misfit between the measured field and the field predicted by the model using as control parameters the unknown model parameters.

In this work, the wave propagation in a waveguide is modelled via the parabolic approximation and a non-local boundary condition in the form of a Neumann to Dirichlet map is used. An Optimal Control Method using the Adjoint Operator of the problem is exhibited for recovering the properties of the medium.

**Acknowledgements**

First, I would like to thank John S. Papadakis, Professor Emeritus of the *Department of Mathematics* of the *University of Crete* and former Director at the *Institute of Applied and Computational Mathematics* (IACM) in the *Foundation for Research and Technology* (FORTH), for the support and the patience.

Next, I would like to thank Michael Taroudakis, Professor at the *Department of Mathematics* of the *University of Crete* and Researcher at IACM in FORTH, for the permission to join the postgraduate program, the support and the advice, as well as George Makrakis, Associate Professor at the *Department of Applied Mathematics* of the *University of Crete* and Researcher at IACM in FORTH, for the support and the advice.

I would also like to thank Evangelia Flouri, Technical Scientist at IACM in FORTH and Ph.D. Candidate in the *Department of Environmental Engineering* of the *Technical University of Crete*, for the patience, support and advice.

This work was carried out at IACM in FORTH.

This is to certify that the thesis comprises only my original work except where indicated in the preface; due acknowledgment has been made in the text to all other material used.

# Contents

# List of Figures

# List of Tables

# Chapter 1

# Introduction

Inverse problems arise in a variety of fields such as medical imaging, electromagnetic tomography, remote sensing, characterization of materials, seismology, meteorology, geophysics, computational fluid dynamics and underwater acoustics.

According to [20], a fundamental step in the solution of most non-linear inverse problems is to establish a relationship between changes in the adopted model and resulting changes in the forward modelled data. Once this relationship has been established, we can refine an initial model in order to obtain an improved fit to the observed data. In linearized analysis, the Fréchet derivative is the connecting link between changes in the model and changes in data, i.e. evaluate quantitatively how a change in the model affects the data. There are various techniques, e.g., standard perturbation method, sensitivity-equation method, adjoint-equation method, etc., to derive an analytic expression for the Fréchet derivative. However, for more complicated problems it is necessary to parameterize the model and solve numerically for the sensitivities, i.e. partial derivatives of the data with respect to a finite number of model parameters.

An optimal control approach to the solution of the inverse problem requires the definition of a global error functional which quantifies the discrepancy between

the measured data and the data predicted by the model, [24], [25]. The objective is to minimize the error functional, with the unknown model parameters playing the role of control parameters. The functional gradient (Fréchet derivative) of the global error with respect to the unknown parameters is coupled to an iterative scheme so as to indicate in what direction to update the model parameters in order to reduce the global error at each iteration. In other words, the gradient points "downhill" on the error surface in a multidimensional parameter space, and we seek the minimum by iteratively descending on this surface. The steepest descent or the conjugate-gradient (quasi-Newton) algorithm can be implemented for this purpose. The point is to compute the functional gradient of the error.

A brute force approach to compute the gradient is to vary the unknown parameters in some systematic way and compute the resulting change in the error, e.g., for a finite number of unknown parameters (say $N$), the partial derivatives of the error with respect to the $N$ parameters can be estimated by finite differences. This requires at least $N$ solutions by the forward model per iteration.

Adjoint method gives an analytically exact expression for the gradient which can be computed by solving numerically two problems per iteration: the forward and the adjoint problem. Therefore, adjoint method reduces round-off error, since it generates derivatives at a point rather than approximating them using finite differences at two points. It is also vastly more efficient, since it is independent of the number of the unknown parameters.

Adjoint method is general and applicable to problems governed by a variety of field equations, time-dependent or time-independent in any number of dimensions, e.g., the electrical potential inverse problem [20], the inverse heat-conduction problem [21], the electromagnetic induction inverse problem [22],[23], the inverse transport problem [24], the inverse wave propagation problem [25], etc. The method is also independent of the geometry, source, boundary conditions or data-acquisition scenarios.

When the global error is driven to a minimum, one obtains the true values of the unknown parameters. Convergence to a local minimum is a possibility, but this can usually be recognized by the gradient vanishing at a location where the global error is not small. When this happens, one can restart the descent algorithm at a new location. Another difficulty comes from the fact that inverse problems are ill-posed, i.e. the solutions are very sensitive to changes in input data resulting from measurement and modelling errors, hence may not be unique. In this case, one can impose *a priori* constraints upon the unknown parameters to face out the problem.

In this work, we suppose that the wave propagation inside a medium is modelled by a well posed mathematical problem. Specifically, the adopted model consists of:

1. the properties of the medium (e.g., density, wave speed, attenuation, etc.)

2. the properties and the location of the source

3. the boundary conditions

4. the propagated field.

We choose to write the above problem in terms of a system of partial differential equations with initial and boundary conditions.

The task of specifying the propagated field when the properties of the medium, the properties and the location of the source as well as the boundary conditions are assumed to be known, is called the **Direct Problem**. We suppose that we can obtain a numerical solution for this problem, using an appropriate model.

On the other hand, an **Inverse Problem** arise when the propagated field is assumed to be known by experimental measurements and the objective is to

recover the properties of the medium, or find the location and the properties of the source, or even determine the boundary conditions.

In chapter 2, we present the forward model we will use in this work for the inversion: the wave propagation in a waveguide is modelled via the parabolic approximation and a non-local boundary condition in the form of a Neumann to Dirichlet map is used. In chapter 3, an optimal control method using the adjoint operator of the problem is exhibited for recovering the properties (sound speed, density and attenuation) of the medium, given a set of observations along a vertical array. Three cost functions independent of the source strength are introduced. Two of them are the most interesting, since they make use of the amplitude of the observed field, only, and thus avoid errors due to inherent noise in the measurements. In chapter 4, an illustration is attempted from the field of underwater acoustic propagation. Adjoint method coupled to the steepest-descent algorithm deals with experimental data and convergence to the true values of the unknown parameters is achieved.

# Chapter 2

# The Direct problem

In this chapter we present the model we adopt for the wave propagation in a waveguide. In section 2.1 we derive the Parabolic Equation approximation method that the model is based on. In section 2.2 the model is constructed and the direct problem is given in terms of an initial boundary value problem. The way we obtain a numerical solution for the direct problem is described in section 2.3.

## 2.1 The Parabolic Approximation

In the twentieth century, an important contribution to the modelling of wave propagation prediction is the Parabolic Equation (PE) approximation method. PE models energy propagating in a cone centered on the paraxial direction.

According to [1], [2] and [3], it was Leontovich and Fock, who first applied the method to the problem of radio wave propagation in the atmosphere, in the mid-1940's, in order to calculate the diffraction caused by the spherical shape of the earth. The method was rapidly extended to more complicated cases involving

atmospheric refraction. Still in the 1940's, Malyuzhinets combined the parabolic approximation method with geometrical optics to develop a powerful theory of diffraction by obstacles. Russian workers pioneered the idea of simplifying the wave equation for certain types of radio waves propagation problems and solved a number of these problems in terms of special functions. The method was applied to many other diffraction problems, such as high frequency scattering by obstacles of various shapes. It has also been extensively applied to the theory of microwave, resonators, waveguides, and antennas.

In the early 1960's when coherent sources of optical radiation (lasers) were developed, PE method was naturally adopted for problems of laser beam propagation. In this field, the PE is called the "quasi-optical" equation. In nonlinear optics where the index of refraction depends on the intensity, parabolic method gives an equation known as "nonlinear Schroedinger" equation. The PE method has also been applied to nonlinear optical pulse propagation in dielectric fibers.

Since about 1968, the parabolic method has been extensively used to study the abstract problem of beam propagation in random media. The beams may consist of radio waves (radars), acoustic waves (sonars), optical waves (lasers), and so forth. This problem is equivalent to the quantum mechanical problem of the motion of a particle in a random potential, and has been investigated by many scientists and applied mathematicians.

In 1970's, parabolic equations were used in several branches of physics, such as water wave propagation, optics, seismics, underwater acoustics and latter, in plasma physics. The progress of digital computers open the way for scientists to search numerical solutions rather than closed-form expressions. In 1973, Hardin and Tappert introduced the very efficient split-step Fourier algorithm, based on fast Fourier transforms, for the solution of the PE, whereas Claerbout developed finite-difference codes for geophysics applications. Many workers in the field of underwater acoustics took up the PE method and huge advances were made. PE

approximation has been proven to be a very effective model for computer implementation in a variety of fields and has been derived to deal with complicated problems such as acoustic wave propagation in poro-elastic media or optics in anisotropic waveguides.

Since then, interest in PE techniques has grown steadily, to the point that now it is widely known that PE computer models give fast and accurate results to a large class of problems.

For the following subsections, we will be based on [1], [4] and [5].

### 2.1.1 Derivation of Helmholtz Equation from the Wave Equation

Starting from the hyperbolic type, homogeneous wave equation, in Cartesian coordinates, which describes the wave propagation inside a medium of constant density

$$\nabla^2 P(\mathbf{x},t) - \frac{1}{c^2(\mathbf{x})}\frac{\partial^2}{\partial t^2} P(\mathbf{x},t) = 0, \quad \mathbf{x} = (x,y,z),\ t > 0 \tag{2.1}$$

and considering a point harmonic source of time-dependence $e^{-i\omega t}$, we obtain the elliptic type, time-independent, Helmholtz equation

$$\nabla^2 p(\mathbf{x}) + \frac{\omega^2}{c^2(\mathbf{x})}\, p(\mathbf{x}) = 0, \tag{2.2}$$

where $P(\mathbf{x},t) = p(\mathbf{x})\, e^{-i\omega t}$ is the propagated field, $\rho$ is the density of the medium, $c$ is the propagation speed of the wave and $\omega$ is the circular frequency of the source. It should be noted that $c$ is time-independent, in other words we suppose that the temporal variations of the medium are slow relative to the propagation of the wave.

Assuming that the wave phenomenon is taking place in an axially symmetric

environment, we can write Eq. (2.2) in cylindrical coordinates as

$$\frac{\partial^2}{\partial r^2}\, p(r,z) + \frac{1}{r}\frac{\partial}{\partial r}\, p(r,z) + \frac{\partial^2}{\partial z^2}\, p(r,z) + k_0^2\, n^2(r,z)\, p(r,z) = 0, \tag{2.3}$$

where $z$ is the depth measured vertically, $r$ is the range measured horizontally, $k_0 = \omega/c_0$ is the reference wave number, $c_0$ is the reference propagation speed and $n(r,z) = c_0/c(r,z)$ is the index of refraction.

### 2.1.2 From an Elliptic to a Parabolic Equation

Following Tappert [1], we can assume that the solution of Eq. (2.3) takes the form

$$p(r,z) = H_0^{(1)}(k_0 r)\, u(r,z), \tag{2.4}$$

where $u(r,z)$ is an envelope function, slowly varying in range $r$ and $H_0^{(1)}(k_0 r)$ is the zeroth order Hankel function of the first kind which satisfies the Bessel differential equation

$$\frac{\partial^2 H_0^{(1)}}{\partial r^2} + \frac{1}{r}\frac{\partial H_0^{(1)}}{\partial r} + k_0^2 H_0^{(1)} = 0. \tag{2.5}$$

Substituting Eq. (2.4) into Eq. (2.3) and making use of Eq. (2.5), we obtain

$$\frac{\partial^2 u}{\partial r^2} + \left(\frac{2}{H_0^{(1)}}\frac{\partial H_0^{(1)}}{\partial r} + \frac{1}{r}\right)\frac{\partial u}{\partial r} + \frac{\partial^2 u}{\partial z^2} + k_0^2(n^2-1)u = 0. \tag{2.6}$$

Using, next, the asymptotic form of the Hankel function for $k_0 r \gg 1$,

$$H_0^{(1)}(k_0 r) \approx \sqrt{\frac{2}{\pi k_0 r}}\, e^{i(k_0 r - \frac{\pi}{4})}$$

and observing that

$$\frac{\partial H_0^{(1)}}{\partial r} = H_0^{(1)}\frac{2ik_0 r - 1}{2r} \approx H_0^{(1)} k_0 i, \quad \text{for } k_0 r \gg 1,$$

Eq. (2.6) gives the simplified elliptic equation

$$\frac{\partial^2 u}{\partial r^2} + 2ik_0\frac{\partial u}{\partial r} + \frac{\partial^2 u}{\partial z^2} + k_0^2(n^2-1)u = 0. \tag{2.7}$$

If we define the two operators as in [4] and [5]

$$P = \frac{\partial}{\partial r}, \quad Q = \sqrt{n^2 + \frac{1}{k_0^2}\frac{\partial^2}{\partial z^2}},$$

Eq. (2.7) becomes

$$(P^2 + 2ik_0P + k_0^2(Q^2 - 1))u = 0 \tag{2.8}$$

which is factored as follows

$$(P + ik_0 - ik_0Q)(P + ik_0 + ik_0Q)u - ik_0(PQ - QP)u = 0. \tag{2.9}$$

We observe that for range-independent media where $n = n(z)$, $PQ \equiv QP$. Hence, ignoring the last term of Eq. (2.9) and selecting only the outgoing wave component we take

$$Pu = ik_0(Q - 1)u$$

or

$$\frac{\partial u}{\partial r} = ik_0\left(\sqrt{n^2 + \frac{1}{k_0^2}\frac{\partial^2}{\partial z^2}} - 1\right)u. \tag{2.10}$$

Eq. (2.10), known as the **General Parabolic Equation (GPE)**, is a non-local parabolic approximation to Helmholtz' s equation. It is important to note that GPE is exact within the limits of the far-field approximation ($k_0r \gg 1$), for range-independent environments where only one-way wave propagation is present. In the sequel, we assume that the range-dependence of $n(r, z)$ is weak enough that we can ignore the term $ik_0(PQ - QP)u$ and backscattering is negligible enough that we can keep only the outgoing waves.

GPE is the basis for obtaining various forms of parabolic approximations, i.e. partial differential equations in first order with respect to $r$. Indeed, there exist an infinity of parabolic approximations to the elliptic equation. In the sequel, we will present those which are preferable in numerical implementations.

### Rational Linear PE approximations

First, we write the square-root operator of the GPE in the form

$$\sqrt{1+q}, \quad \text{where} \quad q = n^2 + \frac{1}{k_0^2}\frac{\partial^2}{\partial z^2} - 1.$$

It can be proven that the operator $q$ is a function of the source radiation angle. Rational-function approximations to the square-root operator are given by

$$\sqrt{1+q} \approx \frac{a_0 + a_1 q}{b_0 + b_1 q}, \tag{2.11}$$

where the coefficients $a_0$, $a_1$, $b_0$ and $b_1$ can be chosen so as to minimize the error over a given angle interval. We give, below, two common paraxial approximations:

- If we choose $a_0 = 1$, $a_1 = 0.5$, $b_0 = 1$ and $b_1 = 0$ we obtain the following approximation

  $$\sqrt{1+q} \approx 1 + 0.5q.$$

  Substituting this expression for the square-root operator into the GPE, Eq. (2.10), we arrive at a PE of the form

  $$2ik_0 u_r + u_{zz} + k_0^2(n^2 - 1)u = 0, \tag{2.12}$$

  which is known as the **Narrow-Angle** or **Standard PE (SPE)**. SPE is considered accurate only for propagation angles within $10 - 15^\circ$ off the horizontal. A two-term Taylor expansion of the square-root operator around $q = 0$ can also lead to this approximation, since $q$ is small for propagation near the horizontal.

- Selecting $a_0 = 1$, $a_1 = 0.75$, $b_0 = 1$ and $b_1 = 0.25$ yields

  $$\sqrt{1+q} \approx \frac{1 + 0.75q}{1 + 0.25q},$$

  which leads to the **Wide-Angle PE (WAPE)**

  $$2ik_0\left[1 + \frac{1}{4}(n^2 - 1)\right]u_r + u_{zz} + k_0^2(n^2 - 1)u + \frac{i}{2k_0}u_{rzz} = 0, \tag{2.13}$$

  due to Claerbout. WAPE is valid for propagation angles up to about $40^\circ$.

### 2.1.3 Elliptic versus Parabolic

The principal advantage of the parabolic wave equation over the elliptic Helmholtz equation is that the PE is a one-way wave equation which can be solved by a range-marching solution technique. Since PE is in first order with respect to $r$, the field is advanced one step at a time in range using only information about the field at previously computed ranges. Furthermore, one solves for the slowly varying envelope function $u(r, z)$ itself, so the computations do not have to be done on the scale of wavelength. Consequently, PE solution is much cheaper to obtain than solving the elliptic Helmholtz equation both in memory and running time savings.

In contrast with the parabolic initial boundary value problem, the elliptic boundary value problem requires a specification of vertical boundaries conditions, around the source. In addition, the usual outgoing radiation condition does not apply to an environment with horizontal variations and therefor difficulties arise when a range-dependent environment with non-horizontal boundaries must be handled. The method most commonly used in this case is the parabolic approximation method.

Nevertheless, we must not forget that PE is an approximation to the elliptic Helmholtz equation and is derived under some assumptions. Thus, it must be kept in mind that the error could be large whenever a PE is used.

## 2.2 The model

It should be useful to recapitulate the assumptions and approximations we have made in section 2.1, since in the sequel, the wave propagation is modelled by the parabolic equation. Firstly, we are in a two dimensional (axially symmetric) environment, where a monochromatic source is located. Inside the propagation

medium the index of refraction can depend on depth but it is strictly weakly range-dependent. Secondly, we make the far-field assumption, in other words, we are interesting in the propagated field at a range much greater than the wavelength. We also neglect the backscattered field. Finally, we assume that the source radiation angle is small.

We can now specify the waveguide, the source and the boundary conditions, in order to obtain a well-posed initial boundary value problem.

### 2.2.1 The Waveguide

In this work, we consider a semi-infinite domain $D = \{0 \leq r < \infty,\ 0 \leq z < \infty\}$, Fig. 2.1, which can consist of $L + 1$, horizontal layers:

- a layer $D_1 = \{0 \leq r < \infty,\ 0 \leq z \leq z_1\}$, of depth $z_1$, constant density $\rho_1$ and propagation speed $c_1(r, z)$ varying in both range $r$ and depth $z$. The index of refraction is $n_1(r, z) = c_0/c_1(r, z)$, where $c_0$ is the reference propagation speed. $n_1$ is assumed to be weakly range-dependent.

- $L - 1$ intermediate layers $D_l = \{0 \leq r < \infty,\ z_{l-1} \leq z \leq z_l\}$ for $l = 2, ..., L$, of constant density $\rho_l$ and propagation speed $c_l$. For the index of refraction we have
$$n_l^2 = \left(\frac{c_0}{c_l}\right)^2 (1 + i\alpha\beta_l)\,,$$
where $\beta_l$ is the attenuation in $D_l$. The thickness of each layer is $d_l = z_l - z_{l-1}$.

- a semi-infinite lower layer $D_{L+1} = \{0 \leq r < \infty,\ z_L \leq z < \infty\}$, of constant density $\rho_{L+1}$ and propagation speed $c_{L+1}$. For the index of refraction we have
$$n_{L+1}^2 = \left(\frac{c_0}{c_{L+1}}\right)^2 (1 + i\alpha\beta_{L+1})\,,$$
where $\beta_{L+1}$ is the attenuation in $D_{L+1}$.

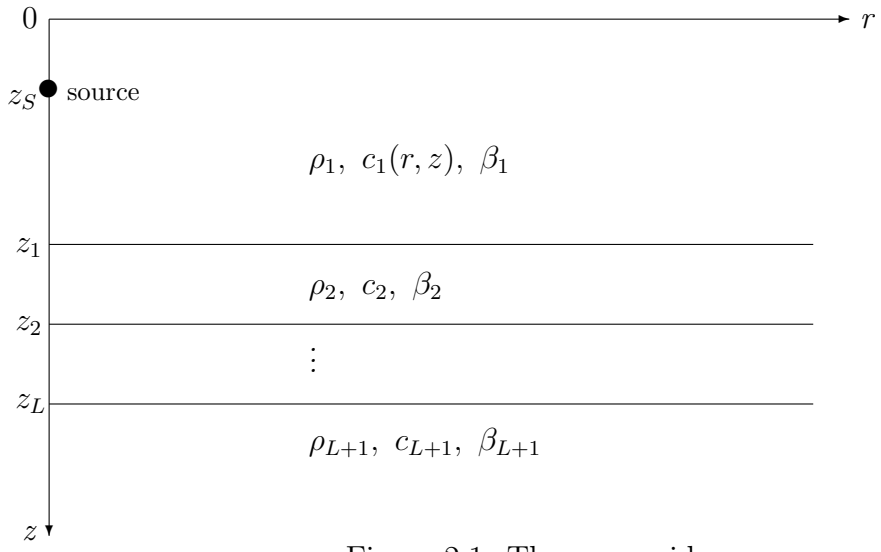


Figure 2.1: The waveguide.

$\alpha$ is a constant depending on the units of the attenuation. Here the attenuation is measured in $dB/$wavelength, so $\alpha = \dfrac{1}{27.287527}$.

The initial field at range $r = 0$ is given by a point harmonic source which is located at range $r = 0$ and depth $z = z_s$ inside $D_1$. We also suppose that at depth $z = 0$ there exist a perfectly reflecting interface, whereas at $z \to \infty$ Sommerfeld radiation condition holds. This means that the energy which is radiated from the source scatters to infinity and no energy may be radiated from infinity into the field.

### 2.2.2 The Source

Analytic or numerical sources can be used in order to model a point source. Particularly, we need a beam-limited source with an aperture that is compatible with the angular limitations of the PE.

A numerical source can be obtained by using as initial data a numerical solution of the elliptic wave equation in a small range containing the source.

In this work we will prefer an analytic source. The analytic source functions

are designed to closely match the far-field result for a point source solution of the Helmholtz equation. For the SPE, Tappert [1] propose a Gaussian source of the form

$$u(0,z) = \sqrt{k_0}\, e^{-k_0^2(z-z_s)^2/2}.$$

However, WPE require a more wide-angle source. According to [5], a good choice is a weighted Gaussian source of the form

$$u(0,z) = \sqrt{k_0}\left(1.4467 - 0.4201k_0^2(z-z_s)^2\right) e^{-k_0^2(z-z_s)^2/3.0512},$$

known as Greene's source.

The perfectly reflecting interface at $z = 0$ produce a negative image of the source and therefore an appropriate initial condition is given by

$$u(0,z) - u(0,z+2z_s).$$

### 2.2.3 The Boundary Conditions

As pointed out in subsection 2.1.3, numerical solutions of a Parabolic Equation are achieved by marching the field in the $r$-direction. The perfectly reflecting interface of the considered waveguide can be simulated by imposing a zero Dirichlet condition at $z = 0$, which is easily implemented in any numerical solution scheme.

The simulation of the lower boundary condition is more complicated, since a semi-infinite problem in the z-direction with a radiation condition at infinity, must be transformed to a problem in a finite domain with an appropriate boundary condition.

Radiation conditions are typically handled with a false layer, [4], [5]. Specifically, a common approach is to add an artificial absorption layer at a depth $z_f$ below the lower interface. The thickness $d_f$ of the absorption layer is given by $d_f = z_c - z_f$. A zero boundary condition is imposed at the computational boundary $z_c$. The absorption layer is usually modelled by introducing an exponentially

increasing with depth in the layer, wave attenuation in the index of refraction. Although $z_c$ must be placed several wavelengths below $z_f$, so as to ensure that no significant energy is reflected from the boundary, there is not a prescribed depth $z_f$, where the artificial absorption layer should be located. Nevertheless, this approach is sufficient for most practical applications.

Correct computational boundary conditions were first introduced by Papadakis in the PE Workshop I (March 1982) [7], in the form of a non-local impedance condition for the SPE. Exact non-local bottom boundary conditions for the WAPE have presented by Papadakis in the PE Workshop II (May 1991) [8] and in [9]. Impedance boundary conditions have also derived for the case of an elastic lower layer, [10], as well as for a slopping lower interface, [11].

In particular, in Papadakis' approach the impedance boundary condition is given in terms of an integral along the lower interface of the semi-infinite domain, or along a computational horizontal interface, below the actual, lower interface. The basic assumption in this approach is that below the interface (actual or computational) the medium is homogeneous. This technique avoids the introduction of an artificial absorption layer and consequently reduces the computational domain as well as the computing time, since the computational boundary is placed at the lower interface or a few $\Delta z$ below this.

Different forms of non-local boundary conditions have also been introduced into the parabolic equations models, [12], [13], [14], [15], [16].

### 2.2.4 Impedance Formulation

In this work, we will make use of a non-local impedance boundary condition, due to Papadakis. We follow the same process as in [7] and [10]. We choose to place the computational boundary at some depth $z = z_c$ with $z_c \geq z_L$, where the impedance condition is imposed on. Doing so, we suppose that the wave

penetrate the intermediate layers $D_l$, for $l = 2, ..., L$ and the reflections come mainly from $D_{L+1}$.

### Derivation of the Impedance Boundary Condition for the SPE

Firstly, we assume that the wave propagation inside the considered waveguide is described by Eq. (2.12) (SPE). Next, we divide the semi-infinite domain $D$ into the interior domain $D^I = \{0 < r < \infty,\ 0 \le z \le z_c\}$ and the exterior domain $D^E = \{0 < r < \infty,\ z \ge z_c\}$. We can write now the continuity conditions that must hold across the interface at $z_c$

$$u^I(r, z_c) = u^E(r, z_c), \quad \frac{1}{\rho_I}\, u^I_z(r, z_c) = \frac{1}{\rho_E}\, u^E_z(r, z_c) \tag{2.14}$$

where $u^I$ and $u^E$, as well as $\rho_I$ and $\rho_E$ are the field and the density in $D^I$ and $D^E$, respectively.

Secondly, we consider the following Fourier transform pair

$$F(\lambda) = \int_{-\infty}^{\infty} e^{-ik_0(\lambda-1)r/2}\, f(r)\, dr, \tag{2.15}$$

$$f(r) = \frac{k_0}{4\pi} \int_{-\infty}^{\infty} e^{ik_0(\lambda-1)r/2}\, F(\lambda)\, d\lambda. \tag{2.16}$$

Applying the transform of Eq. (2.15) to Eq. (2.12) and making use of the following Fourier transform properties

$$\frac{d^n}{dr^n}\, f(r) = \left(\frac{ik_0}{2}\,(\lambda - 1)\right)^n F(\lambda) \quad \text{and} \quad f(r)\, g(r) = (F * G)(\lambda),$$

where $*$ denotes convolution, we obtain

$$U^I_{zz}(\lambda, z) + k_0^2\, (N_I^2 * U^I)(\lambda, z) - k_0^2\, \lambda\, U^I(\lambda, z) = 0, \quad \text{for} \quad z < z_c. \tag{2.17}$$

$$U^E_{zz}(\lambda, z) + k_0^2\, (n_E^2 - \lambda)\, U^E(\lambda, z) = 0, \quad \text{for} \quad z \ge z_c. \tag{2.18}$$

where $N_I^2(\lambda, z)$, $U^I(\lambda, z)$ and $U^E(\lambda, z)$ is the Fourier transform of $n_I^2(r, z)$, $u^I(r, z)$ and $u^E(r, z)$, respectively. $n_I$ and $n_E$ is the index of refraction in $D^I$ and $D^E$, respectively.

The solution of Eq. (2.18) which satisfies the radiation condition at $z \to \infty$ is given by

$$U^E(\lambda, z) = A(\lambda)\, e^{ik_0(n_E^2-\lambda)^{1/2}z}. \tag{2.19}$$

By applying the transform to the Eqs. in (2.14) and then taking the quotient of the two equations, we obtain

$$\frac{U_z^I(\lambda, z_c)}{\rho_I U^I(\lambda, z_c)} = \frac{U_z^E(\lambda, z_c)}{\rho_E U^E(\lambda, z_c)}. \tag{2.20}$$

Finally, the substitution of $U^E(\lambda, z_c)$ and $U_z^E(\lambda, z_c)$ by the Eq. (2.19) in Eq. (2.20), leads to the impedance condition

$$U^I(\lambda, z_c) = -\frac{i}{k_0}\frac{\rho_E}{\rho_I}\,(n_E^2 - \lambda)^{-1/2}\, U_z^I(\lambda, z_c). \tag{2.21}$$

Applying now the inverse transform to Eq. (2.21) we get

$$u(r, z_c) = -\frac{i}{4\pi}\frac{\rho_E}{\rho_I}\int_{-\infty}^{\infty} e^{ik_0(\lambda-1)r/2}\,(n_{L+1}^2 - \lambda)^{-1/2}\, U_z(\lambda, z_c)\, d\lambda, \tag{2.22}$$

where we have dropped the superscript $^I$, $\rho_E$ and $n_E$ have been replaced by $\rho_{L+1}$ and $n_{L+1}$, the density and the index of refraction of the lower layer, respectively, whereas $\rho_I$ is given by

$$\rho_I = \begin{cases} \rho_L, & \text{if } z_c = z_L; \\ \rho_{L+1}, & \text{if } z_c > z_L. \end{cases}.$$

Using the transform representation of $U_z(\lambda, z_c)$, interchanging the order of integration and taking into account that $u(r, z_c) = 0$ for $r \le 0$, Eq. (2.22) gives

$$u(r, z_c) = -\frac{i}{4\pi}\frac{\rho_{L+1}}{\rho_I}\int_0^r u_z(s, z_c)\int_{-\infty}^{\infty} e^{ik_0(\lambda-1)(r-s)/2}\,(n_{L+1}^2 - \lambda)^{-1/2}\, d\lambda\, ds. \tag{2.23}$$

Making use of the Fourier integral tables in [17] for the inside integral of Eq. (2.23), we get

$$u(r, z_c) = \int_0^r u_z(s, z_c)\, G(r - s, z_c)\, ds, \tag{2.24}$$

where

$$G(r - s, z_c) = -\sqrt{\frac{i}{2\pi k_0}}\frac{\rho_{L+1}}{\rho_I}\, e^{ik_0(n_{L+1}^2-1)(r-s)/2}\,(r - s)^{-1/2}, \tag{2.25}$$

which is the desired impedance condition for the problem. This condition gives the field at a range $r$ on the computational interface at $z_c$ in terms of its normal derivative, multiplied by a phase factor depending on the characteristics of $D^E$, and integrated along the computational interface, from range zero to the present range.

In [8], Papadakis applies the impedance boundary condition for the SPE to the WAPE boundary value problem with excellent results. This is justified by the fact that both SPE and WAPE are approximations to the GPE. In the sequel we will follow this combination for convenience, since the derivative of $G$ with respect to the unknown parameters must be calculated for the inversion.

### 2.2.5 The Initial Boundary Value Problem

We can write now, the well posed initial boundary value problem, modelling the wave propagation in the waveguide of Fig. 2.1, in the operator form

$$\left.\begin{aligned} Lu = 2ik_0\Big[1+\frac{1}{4}\,(n^2-1)\Big]u_r + u_{zz} + k_0^2(n^2-1)u + \frac{i}{2k_0}\,u_{rzz} = 0 \\ u(0,z) = S(z,z_S), \quad \text{source condition at } z = z_S \\ u(r,0) = 0, \quad \text{surface condition} \\ u(r,z_c) = \int_0^r u_z(s,z_c)\,G(r-s,z_c)\,ds \quad \text{for } z = z_c \end{aligned}\right\} \tag{2.26}$$

where $S(z,z_S)$ is the Greene's source described in subsection 2.2.2.

The non-local boundary condition along the computational boundary at $z = z_c$ above, is called Neumann to Dirichlet (NtD) map because it is in the form of a convolution integral. The kernel $G(r-s,z_c)$ is the restriction of the Greene's function, of the parabolic operator in the region $\{0 < r < \infty,\ z \geq z_c\}$, along the computational boundary at $z = z_c$. As we justified in subsection 2.2.4, in the sequel we assume that the parabolic operator in this region, is the standard parabolic operator, hence $G$ is given by Eq. (2.25).

## 2.3 Numerical Implementation

A variety of finite-difference schemes (explicit or implicit) can be applied to the parabolic wave equation. Implicit finite-difference methods are faster than explicit ones. They are also unconditionally stable. IFD code developed by Lee and Botseas [18] implements an implicit finite-difference scheme and gives accurate numerical solutions for both narrow and wide angle PE. The Impedance boundary condition for the SPE, due to Papadakis, has been incorporated in the IFD code, [19]. The parabolic code used in this work is the latest version of the IFD+Impedance code developed at IACM in FORTH. This code implements impedance boundary conditions for both SPE and WAPE.

For the following subsections, we will be based on [5].

### 2.3.1 Interface Treatment

The correct treatment of wave reflection and transmission at the horizontal interfaces of a stratified medium with density, propagation speed and attenuation contrasts is of paramount importance to a realistic modelling of propagation in a waveguide.

We consider the far-field Helmholtz equation given by Eq. (2.7). The continuity conditions that must hold across the interfaces at $z_l$ are

$$u^l(r, z_l) = u^{l+1}(r, z_l), \quad \frac{1}{\rho_l} u_z^l(r, z_l) = \frac{1}{\rho_{l+1}} u_z^{l+1}(r, z_l), \quad \text{for} \quad l = 1, ..., L. \quad (2.27)$$

$L$ is the number of the horizontal interfaces separating the medium, see Fig. 2.1.

We next define the computational domain $D_{comp} = \{0 \leq r \leq R,\ 0 \leq z \leq z_c\}$ and discretize it in $N \times M$ equal grids of dimension $\Delta r \times \Delta z$, so that $r = n\Delta r$, for $n = 0, ..., N$ and $z = m\Delta z$, for $m = 0, ..., M$. Note that $R = N\Delta r$ is the max range and $z_c = M\Delta z$ is the max computational depth. We also define $M_l$ so that

$z_l = M_l \Delta z$, for $l = 1, ..., L$.

$\underline{\mathbf{D_l}}$: The field $u^l(r, z_l)$ in $D_l$ on the interface at $z = z_l$ satisfies Eq. (2.7)

$$\frac{\partial^2 u^l}{\partial r^2} + 2ik_0 \frac{\partial u^l}{\partial r} + \frac{\partial^2 u^l}{\partial z^2} + k_0^2 (n_l^2 - 1) u^l = 0. \tag{2.28}$$

Denoting $u^l$ by $u^n_{M_l}$, we can introduce a Taylor series expansion of $u^n_{M_l-1}$ upon $u^n_{M_l}$

$$u^n_{M_l-1} = u^n_{M_l} - \Delta z \frac{\partial u^n_{M_l}}{\partial z} + \frac{(\Delta z)^2}{2} \frac{\partial^2 u^n_{M_l}}{\partial z^2} + ...$$

and solve for the second derivative of $u^l$ to obtain

$$\frac{\partial^2 u^l}{\partial z^2} = -\frac{2}{(\Delta z)^2} (u^l - u^n_{M_l-1}) + \frac{2}{\Delta z} \frac{\partial u^l}{\partial z}.$$

Substituting the above expression for the second derivative in Eq. (2.28) we can write

$$\frac{\partial u^l}{\partial z} = -\frac{\Delta z}{2} \left[ \frac{\partial^2 u^l}{\partial r^2} + 2ik_0 \frac{\partial u^l}{\partial r} + k_0^2 (n_l^2 - 1) u^l - \frac{2}{(\Delta z)^2} (u^l - u^n_{M_l-1}) \right]. \tag{2.29}$$

$\underline{\mathbf{D_{l+1}}}$: Let $u^{l+1}(r, z_l)$ be the field on the interface at $z = z_l$, in $D_{l+1}$. If we introduce a Taylor series expansion of $u^n_{M_l+1}$ upon $u^n_{M_l}$, such that

$$u^n_{M_l+1} = u^n_{M_l} + \Delta z \frac{\partial u^n_{M_l}}{\partial z} + \frac{(\Delta z)^2}{2} \frac{\partial^2 u^n_{M_l}}{\partial z^2} + ...$$

or

$$\frac{\partial^2 u^{l+1}}{\partial z^2} = \frac{2}{(\Delta z)^2} (u^n_{M_l+1} - u^{l+1}) - \frac{2}{\Delta z} \frac{\partial u^{l+1}}{\partial z},$$

it is easy to derive for $u^{l+1}$ a similar equation as above.

$$\frac{\partial u^{l+1}}{\partial z} = \left[ \frac{\partial^2 u^{l+1}}{\partial r^2} + 2ik_0 \frac{\partial u^{l+1}}{\partial r} + k_0^2 (n_{l+1}^2 - 1) u^{l+1} + \frac{2}{(\Delta z)^2} (u^n_{M_l+1} - u^{l+1}) \right] \times \frac{\Delta z}{2}. \tag{2.30}$$

In order to satisfy the interface conditions in Eqs. (2.27), we require that $u^l = u^{l+1} = u$ in Eqs. (2.29) and (2.30). Next we multiply Eq. (2.29) by $\frac{1}{\rho_l}$ and Eq. (2.30) by $\frac{1}{\rho_{l+1}}$ and equate the two right-hand-sides to obtain

$$\frac{\partial^2 u}{\partial r^2} + 2ik_0\frac{\partial u}{\partial r} - k_0^2 u + \frac{\rho_{l+1}}{\rho_l + \rho_{l+1}}\left(n_l^2 + \frac{\rho_l}{\rho_{l+1}}\, n_{l+1}^2\right)k_0^2 u$$

$$+ \frac{2}{(\Delta z)^2}\,\frac{\rho_{l+1}}{\rho_l + \rho_{l+1}}\left(u^n_{M_l-1} - \frac{\rho_l + \rho_{l+1}}{\rho_{l+1}}\, u^n_{M_l} + \frac{\rho_l}{\rho_{l+1}}\, u^n_{M_l+1}\right) = 0 \quad (2.31)$$

This is the far-field Helmholtz equation valid along the horizontal interfaces at $z = z_l$, for $l = 1, ..., L$. Inside the layers where $n$ and $\rho$ are constant, Eq. (2.31) reduces to

$$\frac{\partial^2 u^2}{\partial r^2} + 2ik_0\frac{\partial u^2}{\partial r} + k_0^2(n^2 - 1)u^2 + \frac{u^n_{m-1} - 2u^n_m + u^n_{m+1}}{(\Delta z)^2} = 0,$$

$$\text{for} \quad m = 0, ..., M_1 - 1, M_1 + 1, ..., M_L - 1, M_L + 1, ..., M$$

which is the Eq. (2.7) with the second depth derivative replaced by a central finite-difference form.

If we set

$$\Gamma_{zz} u = \frac{2}{(\Delta z)^2}\,\frac{\rho_{l+1}}{\rho_l + \rho_{l+1}}\left(u^n_{M_l-1} - \frac{\rho_l + \rho_{l+1}}{\rho_{l+1}}\, u^n_{M_l} + \frac{\rho_l}{\rho_{l+1}}\, u^n_{M_l+1}\right),$$

$$n = \frac{\rho_{l+1}}{\rho_l + \rho_{l+1}}\left(n_l^2 + \frac{\rho_l}{\rho_{l+1}}\, n_{l+1}^2\right) - 1$$

and

$$G = k_0^2 n + \Gamma_{zz},$$

we can write Eq. (2.31) in the form

$$\frac{\partial^2 u}{\partial r^2} + 2ik_0\frac{\partial u}{\partial r} + Gu = 0$$

which, with

$$G = k_0^2(Q^2 - 1),$$

is identical to Eq. (2.8). Following the same procedure as in subsection 2.1.2 we can write the one-way wave equation (GPE)

$$\begin{aligned}\frac{\partial u}{\partial r} &= ik_0(Q-1)u \\ &= ik_0\Big(\sqrt{1+q}-1\Big)u,\end{aligned} \tag{2.32}$$

where $q = \dfrac{G}{k_0^2}$ .

### 2.3.2 The Numerical Scheme

IFD code solves Eq. (2.32) using a Crank-Nicolson finite-difference scheme

$$\frac{u^n - u^{n-1}}{\Delta r} = ik_0\Big(\sqrt{1+q}-1\Big)\frac{u^n + u^{n-1}}{2}$$

or

$$\left[1 - \frac{ik_0\Delta r}{2}\left(\sqrt{1+q}-1\right)\right]u^n = \left[1 + \frac{ik_0\Delta r}{2}\left(\sqrt{1+q}-1\right)\right]u^{n-1}.$$

A rational-function approximation to the square-root operator is used, given by Eq. (2.11). Taking into account the definition of $q$, assuming that the operator $b_0+b_1(n+\dfrac{\Gamma_{zz}}{k_0^2})$ remains constant across a range step, making use of the expressions for $\Gamma_{zz}$ and $n$, and after some calculations, we obtain

$$u^n_{M_l-1} + Xu^n_{M_l} + Ru^n_{M_l+1} = \frac{w_2}{w_2'}\left(u^{n-1}_{M_l-1} + Yu^{n-1}_{M_l} + Ru^{n-1}_{M_l+1}\right) \tag{2.33}$$

where

$$X = \frac{\rho_l + \rho_{l+1}}{\rho_{l+1}}\left[\frac{k_0^2(\Delta z)^2}{2}\left(\frac{w_1'}{w_2'}\right) - 1\right] + \frac{k_0^2(\Delta z)^2}{2}\left[(n_l^2 - 1) + \frac{\rho_l}{\rho_{l+1}}\left(n_{l+1}^2 - 1\right)\right],$$

$$Y = \frac{\rho_l + \rho_{l+1}}{\rho_{l+1}}\left[\frac{k_0^2(\Delta z)^2}{2}\left(\frac{w_1}{w_2}\right) - 1\right] + \frac{k_0^2(\Delta z)^2}{2}\left[(n_l^2 - 1) + \frac{\rho_l}{\rho_{l+1}}\left(n_{l+1}^2 - 1\right)\right],$$

$$R = \frac{\rho_l}{\rho_{l+1}}$$

and

$$w_1 = b_0 + \frac{ik_0\Delta r}{2}(a_0 - b_0),$$
$$w_1' = b_0 - \frac{ik_0\Delta r}{2}(a_0 - b_0),$$
$$w_2 = b_1 + \frac{ik_0\Delta r}{2}(a_1 - b_1),$$
$$w_2' = b_1 - \frac{ik_0\Delta r}{2}(a_1 - b_1).$$

We can complete the IFD formulation if we extend the solution given by Eq. (2.33) and collect the solution over $M$ mesh points in depth, into a global matrix solution

$$\begin{bmatrix} X_1 & R_1 & & & & & \\ 1 & X_2 & R_2 & & & & \\ & \ddots & \ddots & \ddots & & & \\ & & & 1 & X_{M-2} & R_{M-2} & \\ & & & & 1 & X_{M-1} & \end{bmatrix} \begin{bmatrix} u_1 \\ u_2 \\ \vdots \\ u_{M-2} \\ u_{M-1} \end{bmatrix}^n + \begin{bmatrix} u_0 \\ 0 \\ \vdots \\ 0 \\ u_M \end{bmatrix}^n$$
$$= \left(\frac{w_2}{w_2'}\right) \begin{bmatrix} Y_1 & R_1 & & & & \\ 1 & Y_2 & R_2 & & & \\ & \ddots & \ddots & \ddots & & \\ & & 1 & Y_{M-2} & R_{M-2} & \\ & & & 1 & Y_{M-1} & \end{bmatrix} \begin{bmatrix} u_1 \\ u_2 \\ \vdots \\ u_{M-2} \\ u_{M-1} \end{bmatrix}^{n-1} + \begin{bmatrix} u_0 \\ 0 \\ \vdots \\ 0 \\ u_M \end{bmatrix}^{n-1} \quad (2.34)$$

where $u_0^{n-1} = u_0^n = 0$, according to the surface condition and $u_M^{n-1}$, $u_M^n$ is the field at $z_c$ in the initial and the advanced range level, respectively. Note that this solution involves two tridiagonal matrices, which can be easily symmetrized by multiplying through row-wise by the appropriate density ratios, i.e. $R_1$ in row 2, $R_2$ in row 3, etc. IFD computer code solves Eq. (2.34) for every step in range, until the max range $R$.

### 2.3.3 Boundary Treatment

This subsection is based on [9], [10] and [19].

In order to incorporate the impedance boundary condition in the above numerical scheme, we make use of the convolution property and write Eq. (2.24) in the form

$$u(r, z_c) = K \int_0^r u_z(r - s, z_c)\, e^{iks}\, s^{-1/2}\, ds, \tag{2.35}$$

where $K = -\sqrt{\dfrac{i}{2\pi k_0}}\dfrac{\rho_{L+1}}{\rho_I}$ and $k = \dfrac{k_0}{2}(n_{L+1}^2 - 1)$.

Discretizing, we have

$$\begin{aligned}
u(n\Delta r, z_c) &= K \sum_{j=0}^{n-1} \int_{j\Delta r}^{(j+1)\Delta r} u_z(n\Delta r - s, z_c)\, e^{iks}\, s^{-1/2}\, ds \\
&\approx K \sum_{j=0}^{n-1} e^{ikj\Delta r}\, u_z((n-j)\Delta r, z_c) \int_{j\Delta r}^{(j+1)\Delta r} s^{-1/2}\, ds \\
&= 2K\sqrt{\Delta r} \sum_{j=0}^{n-1} e^{ikj\Delta r}\, u_z((n-j)\Delta r, z_c)\, (\sqrt{j+1} - \sqrt{j}) \\
&= 2K\sqrt{\Delta r}\, u_z(n\Delta r, z_c) \\
&\quad + 2K\sqrt{\Delta r} \sum_{j=1}^{n-1} e^{ikj\Delta r}\, u_z((n-j)\Delta r, z_c)\, (\sqrt{j+1} - \sqrt{j}).
\end{aligned} \tag{2.36}$$

We suppose that Eq. (2.36) holds in a small neighborhood of the computational interface and specifically for $z_c - \Delta z < z < z_c$, where $\Delta z$ is the depth step. Thus, we obtain a differential equation of the form

$$u_z(n\Delta r, z) - (2K\sqrt{\Delta r})^{-1}\, u(n\Delta r, z) = -\sum_{j=1}^{n-1} e^{ikj\Delta r}\, u_z((n-j)\Delta r, z)\, (\sqrt{j+1} - \sqrt{j}). \tag{2.37}$$

If we multiply the two parts of Eq. (2.37) by $e^{-(2K\sqrt{\Delta r})^{-1} z}$ and then integrate from $z_c - \Delta z$ to $z_c$ we obtain

$$\begin{aligned}
u_z(n\Delta r, z_c) &= e^{(2K\sqrt{\Delta r})^{-1}\Delta z}\, u(n\Delta r, z_c - \Delta z) \\
&\quad - e^{(2K\sqrt{\Delta r})^{-1} z_c} \sum_{j=1}^{n-1} e^{ikj\Delta r}\, (\sqrt{j+1} - \sqrt{j}) \\
&\quad \times \int_{z_c - \Delta z}^{z_c} u_z((n-j)\Delta r, z)\, e^{-(2K\sqrt{\Delta r})^{-1} z} dz.
\end{aligned} \tag{2.38}$$

We can approximate the integral in the right-hand side of the Eq. (2.38) by

$$\int_{z_c-\Delta z}^{z_c} u_z((n-j)\Delta r, z)\, e^{-(2K\sqrt{\Delta r})^{-1}z} dz \;\approx\; e^{-(2K\sqrt{\Delta r})^{-1}(z_c-\Delta z/2)}\Delta z \times \frac{u((n-j)\Delta r, z_c) - u((n-j)\Delta r, z_c-\Delta z)}{\Delta z}.$$

Substituting this expression for the integral in Eq. (2.38) we finally take

$$\begin{aligned} u(n\Delta r, z_c) \;=\; & e^{(2K\sqrt{\Delta r})^{-1}\Delta z}\, u(n\Delta r, z_c-\Delta z) \\ & - e^{(4K\sqrt{\Delta r})^{-1}\Delta z} \sum_{j=1}^{n-1} e^{ikj\Delta r}\,(\sqrt{j+1}-\sqrt{j}) \\ & \times [u((n-j)\Delta r, z_c) - u((n-j)\Delta r, z_c-\Delta z)]. \end{aligned}$$

or

$$u_M^n = E1\, u_{M-1}^n - \sqrt{E1}\, SUM1, \tag{2.39}$$

where

$$E1 = e^{(2K\sqrt{\Delta r})^{-1}\Delta z}$$

and

$$SUM1 = \sum_{j=1}^{n-1} e^{ikj\Delta r}\left(\sqrt{j+1}-\sqrt{j}\right)\left(u_M^{n-j} - u_{M-1}^{n-j}\right).$$

We can derive from Eq. (2.34) the following equation

$$u_{M-2}^n + X_{M-1} u_{M-1}^n = \frac{w_2}{w_2'}\left(u_{M-2}^{n-1} + Y_{M-1} u_{M-1}^{n-1}\right) + u_M^{n-1} - u_M^n,$$

which using Eq. (2.39) becomes

$$u_{M-2}^n + (X_{M-1}+E1)\, u_{M-1}^n = \frac{w_2}{w_2'}\left(u_{M-2}^{n-1} + Y_{M-1} u_{M-1}^{n-1}\right) + u_M^{n-1} + \sqrt{E1}\, SUM1$$

and the matrix equation is modified so that it can be solved for the unknown vector $u^n$.

# Chapter 3

# The Inverse Problem

In this chapter the Inverse Problem is manipulated via the Optimal Control Adjoint Method. Specifically, in Section 3.1 the inversion problem is put into the form of an optimization scheme. In Section 3.2 the adjoint problem to the direct problem is formulated, and the necessary adjoint non-local boundary conditions are derived, which also have the form of a NtD map. In Sections 3.3 and 3.4 the tangent linear model and three choices of cost functions are defined which lead to three different initial conditions for the adjoint problem. In Section 3.4 the desired formula for evaluating the gradient of the cost function is derived and an analytic multiple frequency adjoint formulation is attempted. In Section 3.5, the numerical implementation of the inversion scheme is described, for both a single and multiple frequency cases.

This chapter is based on [26] and [27].

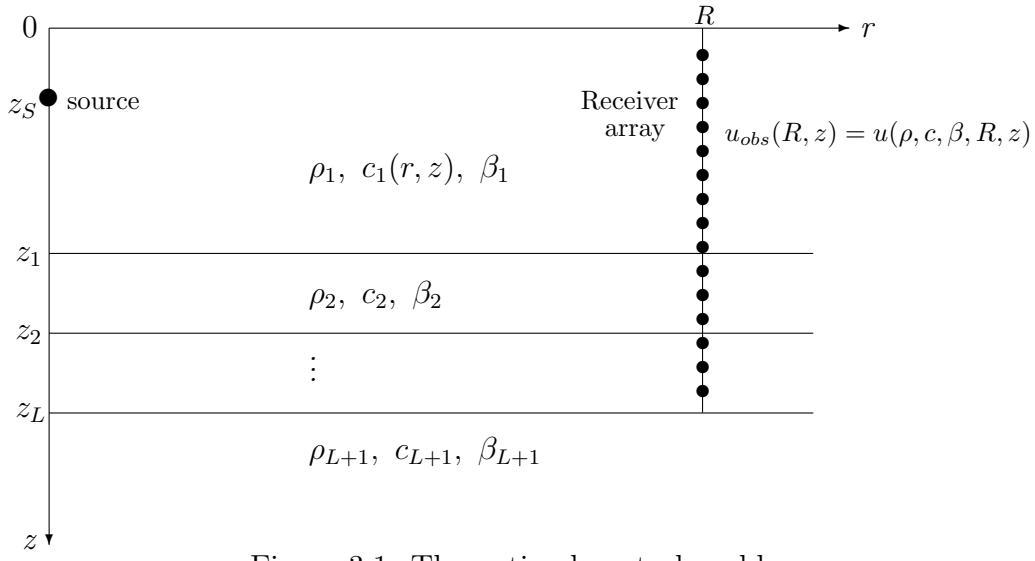


Figure 3.1: The optimal control problem.

## 3.1 The Optimal Control Method

Assume that an experiment is conducted in a waveguide, as in Fig. 3.1, with the objective to recover the parameters $\rho_{L+1}$, $c_{L+1}$ and $\beta_{L+1}$ (density, wave speed and attenuation) of the lower layer from the observed complex field $u_{obs}(R,z)$[1]$= u(\rho_{L+1}, c_{L+1}, \beta_{L+1}, R, z)$ measured by a vertical array of receivers at a range $R$ from the source.

Given an initial guess $(\rho_0, c_0, \beta_0)$ of the parameters of the lower layer, an application of the propagation model of Eq. (2.26) will give the predicted complex field $u(\rho, c, \beta, R, z)$ at the range $R$. At this point a cost function $J(\rho, c, \beta)$ is introduced, which is a measure of the mismatch between the observed field $u_{obs}(R,z)$ and the predicted field $u(\rho, c, \beta, R, z)$.

The task of recovering $\rho_{L+1}$, $c_{L+1}$ and $\beta_{L+1}$ from $u_{obs}$, can be viewed as a control problem, with dynamics the parabolic boundary value problem, the control parameters being $\rho$, $c$ and $\beta$ varying over a compact domain of the Euclidean space and the cost function as defined below.

[1]In the sequel $u_{obs}$ represents the observed parabolic field, i.e. the quotient of the observed field divided by the outgoing Hankel function.

The cost function of a control problem is usually a quadratic function of the difference $u(\rho, c, \beta, R, z) - u_{obs}(R, z)$, so that, in seeking the optimal vector $(\rho_{L+1}, c_{L+1}, \beta_{L+1})$ a minimization process can be applied leading to a local minimum of the function $J(\rho, c, \beta)$.

One choice of $J(\rho, c, \beta)$ is

$$J(\rho, c, \beta) = \frac{1}{2} \int_0^H |u(\rho, c, \beta, R, z) - u_{obs}(R, z)|^2 \, dz \; . \tag{3.1}$$

From the above expression it is clear that

$$J(\rho_{L+1}, c_{L+1}, \beta_{L+1}) = 0 \quad \text{and} \quad \nabla J(\rho_{L+1}, c_{L+1}, \beta_{L+1}) = 0.$$

It can be also observed that in the domains

$$\{\rho, c, \beta \,|\, \rho \geq \rho_{L+1}, \; c \geq c_{L+1}, \; \beta \leq \beta_{L+1}\}$$

and

$$\{\rho, c, \beta \,|\, \rho \leq \rho_{L+1}, \; c \leq c_{L+1}, \; \beta \geq \beta_{L+1}\}$$

as well as in a small neighborhood of $(\rho_{L+1}, c_{L+1}, \beta_{L+1})$,

$$\nabla J(\rho, c, \beta) \geq 0 \quad \text{and} \quad \nabla J(\rho, c, \beta) \leq 0, \quad \text{respectively.}$$

Hence, for each choice of $(\rho, c, \beta)$ in the above neighborhood, if

$$\nabla J(\rho, c, \beta) = \left( \frac{\partial J}{\partial \rho}, \frac{\partial J}{\partial c}, \frac{\partial J}{\partial \beta} \right)$$

could be computed, then $J(\rho, c, \beta)$ could be driven to zero through the sequences

$$\begin{aligned} \rho_{n+1} &= \rho_n - \alpha_\rho \frac{\partial J(\rho_n, c_n, \beta_n)}{\partial \rho} \\ c_{n+1} &= c_n - \alpha_c \frac{\partial J(\rho_n, c_n, \beta_n)}{\partial c} \\ \beta_{n+1} &= \beta_n - \alpha_\beta \frac{\partial J(\rho_n, c_n, \beta_n)}{\partial \beta} \end{aligned} \tag{3.2}$$

where $\alpha = (\alpha_\rho, \alpha_c, \alpha_\beta)$ a scaling factor. As $n \to \infty$, then $\lim_{n\to\infty} \rho_n = \rho_{L+1}$, $\lim_{n\to\infty} c_n = c_{L+1}$ and $\lim_{n\to\infty} \beta_n = \beta_{L+1}$.

The adjoint method enables us to compute $\nabla J(\rho, c, \beta)$ for each choice of $\rho$,$c$,$\beta$ from the direct field $u(\rho, c, \beta, r, z_c)$ and the adjoint field $v(\rho, c, \beta, r, z_c)$.

## 3.2 The Adjoint Problem

We write the operator $L$ of the WAPE in (2.26), in the form

$$Lu = Au_r + u_{zz} + Bu + \frac{i}{2k_0}\, u_{rzz} = 0, \tag{3.3}$$

where $A = 2ik_0\Big[1 + \frac{1}{4}\,(n^2-1)\Big]$ and $B = k_0^2(n^2-1)$. In the sequel the adjoint boundary value problem to the direct problem in (2.26) is formulated, using as inner product

$$(f,g) = \int_0^R \int_0^{z_c} f(r,z)\,\overline{g(r,z)}\,dz\,dr,$$

Applying this inner product in Eq. (3.3), we obtain

$$(Lu, v) = 0. \tag{3.4}$$

Now let $L^\star$ represent the adjoint operator to the operator $L$. $L^\star$ is defined by the following identity

$$(Lu, v) = (u, L^\star v)\,. \tag{3.5}$$

In order to specify $L^\star$, we take the first part of (3.5), integrate by parts and use the surface condition of the direct problem, in (2.26). After some calculations we obtain

$$\begin{aligned}(Lu, v) = (u, L'v) &\\ &+ \int_0^{z_c}\Big(Au + \frac{i}{2k_0}\, u_{zz}\Big)\,\overline{v}\,dz\,\Big|_{r=0}^{R}\\ &+ \int_0^{R}(u_z\overline{v} - u\overline{v}_z)\,dr\,\Big|_{z=z_c}\\ &- \frac{i}{2k_0}\int_0^{R}(u_z\overline{v}_r - u\overline{v}_{rz})\,dr\,\Big|_{z=z_c}\\ &- \int_0^{R}\Big(u_z\overline{v} - \frac{i}{2k_0}\, u_z\overline{v}_r\Big)\,dr\,\Big|_{z=0},\end{aligned} \tag{3.6}$$

where

$$L'v = (A'v)_r + v_{zz} + B'v + \frac{i}{2k_0}\, v_{rzz}$$

and

$$A' = 2ik_0\Big[1 + \frac{1}{4}\left(\overline{n^2} - 1\right)\Big], \quad B' = k_0^2\left(\overline{n^2} - 1\right)$$

or

$$\begin{aligned}(Lu, v) = (u, L'v) \; &+ \text{ Integrals along the lines } r = 0,\ r = R \\ &+ \text{ Boundary integrals along } z = 0,\ z = z_c.\end{aligned}$$

If we choose appropriate conditions, so that the boundary integrals along $z = 0$ and $z = z_c$ in the above equation cancel out, then according to the identity (3.5), $L' \equiv L^\star$.

Firstly, we observe that if we set $v(r, 0) = 0$ as the adjoint surface condition, the integral along $z = 0$ in Eq. (3.6) vanishes. Next, in order to eliminate the first integral along $z = z_c$ in Eq. (3.6) we require

$$\int_0^R u_z \overline{v}\, dr \Big|_{z=z_c} = \int_0^R u \overline{v}_z\, dr \Big|_{z=z_c} \tag{3.7}$$

The substitution of $u(r, z_c)$ in Eq. (3.7) by the non-local boundary condition at $z = z_c$ of the direct problem in (2.26), yields

$$\begin{aligned}\int_0^R u_z(r, z_c)\, \overline{v(r, z_c)}\, dr &= \int_0^R \overline{v_z(r, z_c)} \int_0^r u_z(s, z_c)\, G(r - s, z_c)\, ds\, dr \\ &= \int_0^R \int_s^R \overline{v_z(r, z_c)}\, u_z(s, z_c)\, G(r - s, z_c)\, dr\, ds \\ &= \int_0^R \int_r^R \overline{v_z(s, z_c)}\, u_z(r, z_c)\, G(s - r, z_c)\, ds\, dr \\ &= \int_0^R u_z(r, z_c) \int_r^R \overline{v_z(s, z_c)}\, G(s - r, z_c)\, ds\, dr.\end{aligned}$$

The last equation leads to the adjoint boundary condition

$$v(r, z_c) = \int_r^R v_z(s, z_c)\, \overline{G(s - r, z_c)}\, ds, \tag{3.8}$$

which also has the form of a NtD map.

It is easy to see that choosing this boundary condition for the adjoint problem the second integral along $z = z_c$ of Eq. (3.6) vanishes. Specifically, integrating by

parts we can write this integral in the form

$$-\frac{i}{2k_0}\left[\int_0^R (u_z\overline{v}_r + u_r\overline{v}_z)\,dr\,\Big|_{z=z_c} - u(R,z_c)\overline{v_z(R,z_c)}\right] \tag{3.9}$$

Using the Leibniz integral rule we obtain

$$u_r(r,z_c) = \int_0^r u_z(s,z_c)\,G_r(r-s,z_c)\,ds + u_z(r,z_c)G(0,z_c) \tag{3.10}$$

and

$$v_r(r,z_c) = \int_r^R v_z(s,z_c)\,\overline{G_r(s-r,z_c)}\,ds - v_z(r,z_c)\overline{G(0,z_c)}, \tag{3.11}$$

for the boundary condition of the direct and the adjoint problem respectively. Substituting now $u_r(r,z_c)$ and $v_r(r,z_c)$ in (3.9), by the expressions in Eq. (3.10) and (3.11) respectively, we obtain

$$u(R,z_c)\overline{v_z(R,z_c)} - u(0,z_c)\overline{v_z(0,z_c)}, \tag{3.12}$$

where $u(0,z_c)=0$ and $u(R,z_c)\overline{v_z(R,z_c)}$ is a negligible quantity for our numerical computations.

Hence, the adjoint boundary value problem is formulated as follows

$$\left.\begin{aligned} &L^\star v = A'v_r + v_{zz} + B'v + \frac{i}{2k_0}\,v_{rzz} = 0 \\ &v(r,0) = 0, \quad \text{surface condition} \\ &v(r,z_c) = \int_r^R v_z(s,z_c)\,\overline{G(s-r,z_c)}\,ds \\ &\text{Initial conditions at } r=R,\ 0\le z\le z_c\ , \end{aligned}\right\} \tag{3.13}$$

where we have supposed that $n(r,z)$ is weakly range-dependent, so that $(A'v)_r$ can be written as $A'v_r$. The initial condition will be determined in the sequel so that the optimal control adjoint method will work. We must note that if the index of refraction $n$ is a real number (no attenuation is assumed), then the operator of (3.13) is $L$ itself.

## 3.3 The Tangent Linear Model

Since the objective is to calculate the gradient of $J(\rho, c, \beta)$ with respect to the control variables $\rho$, $c$, $\beta$, from the definition of $J$ we see that we need the directional derivatives of the field $u(\rho, c, \beta, r, z)$ in the direction of the control variables $\rho$, $c$, $\beta$.

We define

$$\frac{\partial u}{\partial p^i} = w^i, \quad \text{for } i = 1, 2, 3$$

where $p^1 = \rho$, $p^2 = c$, $p^3 = \beta$ are the **unknown parameters**.

Taking the directional derivatives of the equations in (2.26) we have

$$\left.\begin{aligned} \frac{\partial Lu}{\partial p^i} = Lw^i + \frac{\partial L}{\partial p^i}\, u = 0 \\ w^i(0, z) = 0, \\ w^i(r, 0) = 0, \\ w^i(r, z_c) = \int_0^r w_z^i(s, z_c)\, G(r - s, z_c)\, ds + \int_0^r u_z(s, z_c)\, g^i(r - s, z_c)\, ds \end{aligned}\right\} \tag{3.14}$$

where

$$g^i = \frac{\partial G}{\partial p^i} \quad \text{and} \quad \frac{\partial L}{\partial p^i} = 0 \quad \text{for} \quad i = 1, 2, 3.$$

If we take the inner product of the first equation in (3.14) we obtain

$$\left(\frac{\partial Lu}{\partial p^i}, v\right) = \Big(Lw^i, v\Big) = 0. \tag{3.15}$$

Taking now the second part of Eq. (3.15), integrating by parts and using the zero surface boundary conditions for $w^i$ and $v$, as well as the zero initial condition for $w^i$, we have

$$\begin{aligned} \Big(Lw^i, v\Big) \;&=\; \Big(w^i, L^\star v\Big) \\ &+ \int_0^{z_c} \Big(Aw^i + \frac{i}{2k_0}\, w_{zz}^i\Big)\overline{v}\, dz \,\Big|_{r=R} \\ &+ \int_0^{R} \Big(w_z^i \overline{v} - w^i \overline{v}_z - \frac{i}{2k_0}\, w_z^i \overline{v}_r + \frac{i}{2k_0}\, w^i \overline{v}_{rz}\Big) dr \,\Big|_{z=z_c}. \end{aligned} \tag{3.16}$$

Substituting Eq. (3.16) in (3.15) and taking into account that $\left(w^i, L^\star v\right) = 0$, we obtain

$$\int_0^{z_c}\left(Aw^i + \frac{i}{2k_0}\, w^i_{zz}\right)\overline{v}\, dz\,\Big|_{r=R} = -\int_0^R\left(w^i_z\overline{v} - w^i\overline{v}_z - \frac{i}{2k_0}\, w^i_z\overline{v}_r - \frac{i}{2k_0}\, w^i_r\overline{v}_z\right)dr\,\Big|_{z=z_c} - \frac{i}{2k_0}\, w(R,z_c)\overline{v_z(R,z_c)}. \tag{3.17}$$

### 3.3.1 Elimination of the directional derivative of the Field

The next step is to eliminate the tangent field $w$, from Eq. (3.17) and express it in terms of $u$ and $v$, the direct and the adjoint field, respectively. Note that $u$ and $v$ can be computed from the model. To accomplish this, we use the adjoint non-local boundary condition, derived in section 3.2 and the non-local boundary condition of the tangent problem. Specifically, we substitute $v(r,z_c)$ and $v_r(r,z_c)$ by Eqs. (3.8) and (3.11), respectively, as well as $w^i(r,z_c)$ by the boundary condition in (3.14). For $w^i_r(r,z_c)$ we use the Leibniz rule

$$w^i_r(r,z_c) = \int_0^r w^i_z(s,z_c)\, G_r(r-s,z_c)\, ds + w_z(r,z_c)G(0,z_c) + \frac{d}{dr}\int_0^r u_z(s,z_c)\, g^i(r-s,z_c)\, ds.$$

Hence the integral along $z = z_c$ of the right-hand side in Eq. (3.17) yields

$$\begin{aligned}
-\Bigg[&\int_0^R w^i_z(r,z_c)\int_r^R \overline{v_z(s,z_c)}\, G(s-r,z_c)\, ds\, dr \\
&-\int_0^R \overline{v_z(r,z_c)}\int_0^r w^i_z(s,z_c)\, G(r-s,z_c)\, ds\, dr \\
&-\int_0^R \overline{v_z(r,z_c)}\int_0^r u_z(s,z_c)\, g^i(r-s,z_c)\, ds\, dr \\
&+\frac{i}{2k_0}\int_0^R w^i_z(r,z_c)\left(\int_r^R \overline{v_z(s,z_c)}\, G_{s-r}(s-r,z_c)\, ds + \overline{v_z(r,z_c)}G(0,z_c)\right)dr \\
&-\frac{i}{2k_0}\int_0^R \overline{v_z(r,z_c)}\left(\int_0^r w^i_z(s,z_c)\, G_{r-s}(r-s,z_c)\, ds + w_z(r,z_c)G(0,z_c)\right)dr \\
&-\frac{i}{2k_0}\int_0^R \overline{v_z(r,z_c)}\,\frac{d}{dr}\int_0^r u_z(s,z_c)\, g^i(r-s,z_c)\, ds\, dr\Bigg].
\end{aligned}$$

We observe that interchanging the order of integration, the first and second term, as well as the fourth and fifth term above, cancel out. So the integral along $z = z_c$ of Eq. (3.17) takes the form

$$\int_0^R \overline{v_z(r, z_c)} \left[ \int_0^r u_z(s, z_c)\, g^i(r - s, z_c)\, ds + \frac{i}{2k_0} \frac{d}{dr} \int_0^r u_z(s, z_c)\, g^i(r - s, z_c)\, ds \right] dr,$$

for $i = 1, 2, 3$.

Finally, if we choose to integrate by parts the second term in the integral of the first part in Eq. (3.17) along $0 \le z \le z_c$ and using the above expression for the integral along $z = z_c$, we get

$$\begin{aligned} \int_0^{z_c} \left( \overline{-A'v - \frac{i}{2k_0} v_{zz}} \right) w^i\, dz \Big|_{r=R} = \int_0^R & \overline{v_z(r, z_c)} \left[ \int_0^r u_z(s, z_c)\, g^i(r - s, z_c)\, ds \right. \\ & \left. + \frac{i}{2k_0} \frac{d}{dr} \int_0^r u_z(s, z_c)\, g^i(r - s, z_c)\, ds \right] dr \\ & - \frac{i}{2k_0} w(R, z_c) \overline{v_z(R, z_c)} \end{aligned} \tag{3.18}$$

which will lead to the initial condition for the adjoint problem as well as the derivative of the cost function.

## 3.4 The choice of the Cost Function

If we define the following inner product

$$(u, v) = \int_0^{z_c} u \overline{v}\, dz \Big|_{r=R},$$

we introduce the following cost functions which are independent of the source strength

- $J(p^1, p^2, p^3) = \frac{1}{2} \left( \|u\|^2 - \left( u, \frac{u_{obs}}{\|u_{obs}\|} \right)^2 \right)$, which we call **Full Projection** cost function.

  Making use of the amplitude of the field only we set

- $J(p^1,p^2,p^3) = \dfrac{1}{2}\left(\|u\|^2 - \left(|u|, \dfrac{|u_{obs}|}{\|u_{obs}\|}\right)^2\right)$, which we call **Amplitude Projection** cost function, and
- $J(p^1,p^2,p^3) = \dfrac{1}{2}\displaystyle\int_0^{z_c}\left(|u| - \frac{\|u\|}{\|u_{obs}\|}|u_{obs}|\right)^2 dz$, which we call **Normalized** $L_1$ cost function and becomes from the common $L_1$ norm

$$J(p^1,p^2,p^3) = \frac{1}{2}\int_0^{z_c}\left(|u| - |u_{obs}|\right)^2 dz.$$

We note that $u = u(p^1,p^2,p^3,R,z)$ and $u_{obs} = u_{obs}(R,z)$.

### 3.4.1 Full Projection cost function

Taking now the derivative of $J$ with respect to $p^i$, for $i = 1,2,3$ we have:

$$\frac{\partial J}{\partial p^i} = \mathrm{Re}\int_0^{z_c} w^i\left[\overline{u} - \frac{\overline{u_{obs}}}{\|u_{obs}\|^2}\,\overline{(u,u_{obs})}\right]dz\Bigg|_{r=R} \tag{3.19}$$

Comparing Eq. (3.18) with Eq. (3.19) we observe that if we choose as initial condition for the Adjoint Problem the solution $v(R,z)$ of the following ordinary differential equation

$$-A'v(R,z) - \frac{i}{2k_0}\,v_{zz}(R,z) = u(R,z) - \frac{u_{obs}(R,z)}{\|u_{obs}(R,z)\|^2}(u(R,z),u_{obs}(R,z)) \tag{3.20}$$

then we can obtain the derivative of $J$ in terms of $u$ and $v$

$$\begin{aligned}\frac{\partial J}{\partial p^i} = \mathrm{Re}\int_0^R \overline{v_z(r,z_c)}\,\Bigg[&\int_0^r u_z(s,z_c)\,g^i(r-s,z_c)\,ds \\ &+ \frac{i}{2k_0}\,\frac{d}{dr}\int_0^r u_z(s,z_c)\,g^i(r-s,z_c)\,ds\Bigg]dr,\end{aligned} \tag{3.21}$$

neglecting $\dfrac{i}{2k_0}\,w(R,z_c)\overline{v_z(R,z_c)}$.

### 3.4.2 Amplitude Projection cost function

The derivative of $J$ with respect to $p^i$, for $i = 1,2,3$ is:

$$\frac{\partial J}{\partial p^i} = \mathrm{Re}\int_0^{z_c} w^i\overline{u}\left[1 - \frac{|u_{obs}|}{|u|\|u_{obs}\|^2}\,(|u|,|u_{obs}|)\right]dz\Bigg|_{r=R}. \tag{3.22}$$

If we choose as initial condition for the Adjoint Problem the solution $v(R,z)$ of the following ordinary differential equation

$$-A'v(R,z) - \frac{i}{2k_0}\, v_{zz}(R,z) = u(R,z)[1 - \frac{|u_{obs}(R,z)|}{|u(R,z)|\|u_{obs}(R,z)\|^2}$$

$$\times \left(|u(R,z)|, |u_{obs}(R,z)|\right)], \quad (3.23)$$

then the derivative of $J$ with respect to $p^i$, for $i = 1,2,3$ is given by the Eq. (3.21).

### 3.4.3 Normalized $L_1$ cost function

The derivative of $J$ with respect to $p^i$, for $i = 1,2,3$ is

$$\frac{\partial J}{\partial p^i} = \mathrm{Re} \int_0^{z_c} w^i \overline{u} \left[\frac{1}{|u|}\left(|u| - \frac{\|u\|}{\|u_{obs}\|}\,|u_{obs}|\right) - \frac{1}{\|u\|\|u_{obs}\|}\right.$$

$$\left. \times \int_0^{z_c} |u_{obs}| \left(|u| - \frac{\|u\|}{\|u_{obs}\|}\,|u_{obs}|\right) dz\right] dz \Bigg|_{r=R}. \quad (3.24)$$

For this case, the initial condition for the Adjoint Problem is given by the solution of the following ordinary differential equation

$$-A'v(R,z) - \frac{i}{2k_0}\, v_{zz}(R,z) = u(R,z) \left[\frac{1}{|u(R,z)|}\, U(R,z) - \frac{1}{\|u(R,z)\|\|u_{obs}(R,z)\|}\right.$$

$$\left. \times \int_0^{z_c} |u_{obs}(R,z)|\, U(R,z) dz\right], \quad (3.25)$$

where

$$U(R,z) = |u(R,z)| - \frac{\|u(R,z)\|}{\|u_{obs}(R,z)\|}\,|u_{obs}(R,z)|.$$

The derivative of $J$ with respect to $p^i$, for $i = 1,2,3$ is given by the Eq. (3.21).

### 3.4.4 Multiple Frequency

We assume now, that we can repeat the experiment described in section 3.1 for a set of different source frequencies. It is believed that when the information

at the receivers becomes from different frequencies, a more reliable and accurate prediction for the unknown parameters can be obtained. Therefor, we use as cost function the summary of the cost functions for each frequency

$$J_{total}(p^1, p^2, p^3) = \sum_{f=1}^{No.of frequencies} J^f(p^1, p^2, p^3),$$

so that the derivative of the cost function with respect to $p^i$, for $i = 1, 2, 3$ is given by

$$\frac{\partial J_{total}}{\partial p^i} = \sum_{f=1}^{No.of frequencies} \frac{\partial J^f}{\partial p^i},$$

where $J^f$ is given by Eq. (3.21) and $f$ indicates the frequency.

## 3.5 Numerical Implementation

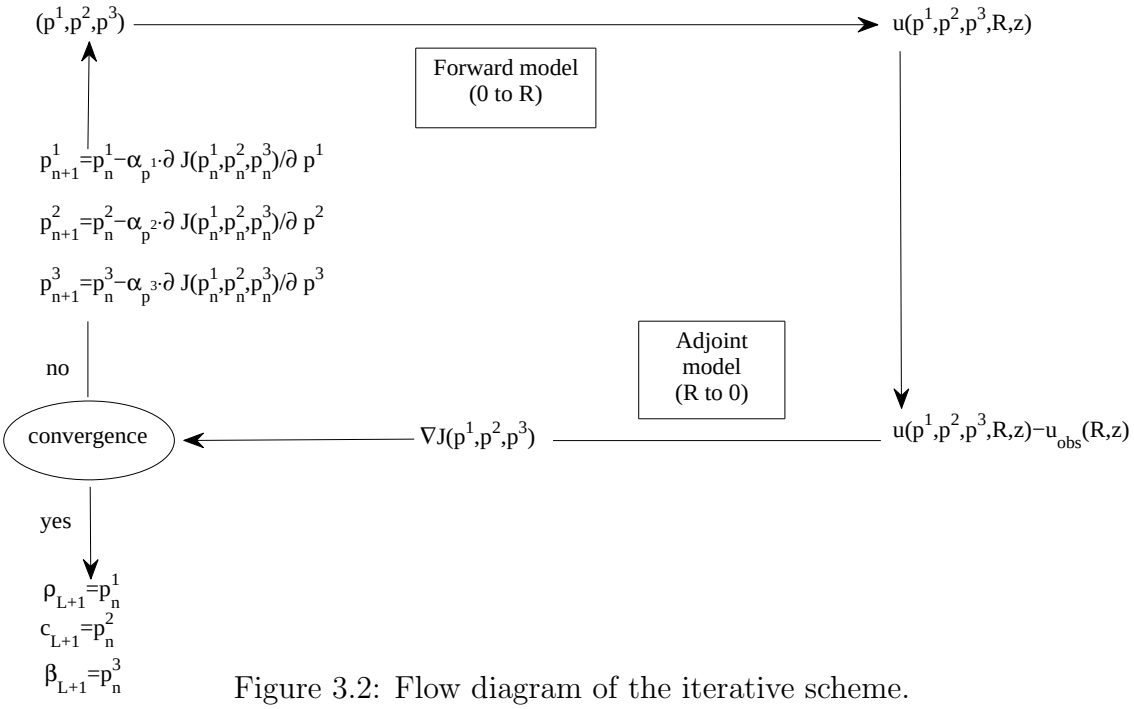


Figure 3.2: Flow diagram of the iterative scheme.

The direct and the adjoint problems are solved numerically by a Crank-Nicolson finite-difference scheme on an Intel Core Duo 3.0GHz, 32bit, PC processor. The parabolic code used is the latest version of the IFD+Impedance code developed at IACM in FORTH.

All the above cost functions have been used for the inversion. The initial field for the adjoint is given by (3.20) for the Full Projection cost function, by (3.23) for the Amplitude Projection cost function and by (3.25) for the Normalized $L_1$ cost function. In order to be able to define it correctly, a full array of receivers at each node of the Crank-Nicolson scheme is needed. However, if the number of receivers is much smaller than the number of nodes, as it is usually the case, then the right-hand side of the differential equations in (3.20), (3.23) and (3.25), is multiplied by a Gaussian source function at each receiver, as it has been defined in [1].

A steepest descent algorithm is implemented: we start with an initial guess $(p_0^1, p_0^2, p_0^3) \equiv (\rho_0, c_0, \beta_0)$ of the parameters of the lower layer. We propagate the field in the $r$–direction. We use Eq. (3.20), (3.23) or (3.25) to find the initial field for the adjoint. We propagate through the adjoint operator backwards in $r$ and compute the $\nabla J(p_0^1, p_0^2, p_0^3)$. We correct the initial guess $p_0^1, p_0^2, p_0^3$ as in Eq. (3.2) and we repeat the process with $p_1^1, p_1^2, p_1^3$. This process is exhibited in the flow diagram in Fig. 3.2.

The algorithm described above has been modified appropriately for the case of a broad range of frequencies: we use the forward and adjoint models in order to compute the $\nabla J(p^1, p^2, p^3)$, for each frequency. The corrections to the unknown parameters are taking place in the direction of $\nabla J_{total}(p^1, p^2, p^3)$.

# Chapter 4

# Numerical Results

In this chapter, we exhibit some examples from the field of underwater acoustic propagation. The main reason for doing so is that at this time the available experimental data are coming from the sea. Nevertheless, we must point out that the Optimal Control Adjoint Method we have developed and used, is derived from a general technique which is applicable to inverse problems of all descriptions, provided only that solutions to the forward and adjoint problems can be found numerically.

## 4.1 Examples

For the following Test Cases, Full Projection cost function gives accurate results for the observed values obtained by the solution of Eq. (2.26), derived by the IFD+Impedance code. However, when we try it with observed values obtained by the solution of the elliptic equation using a Normal Mode code, Full Projection cost function cannot give a minimum. This is justified by the fact that the parabolic approximation changes the phase of the field. For observed values by Experimental measurements where the noise changes the phase, the Full

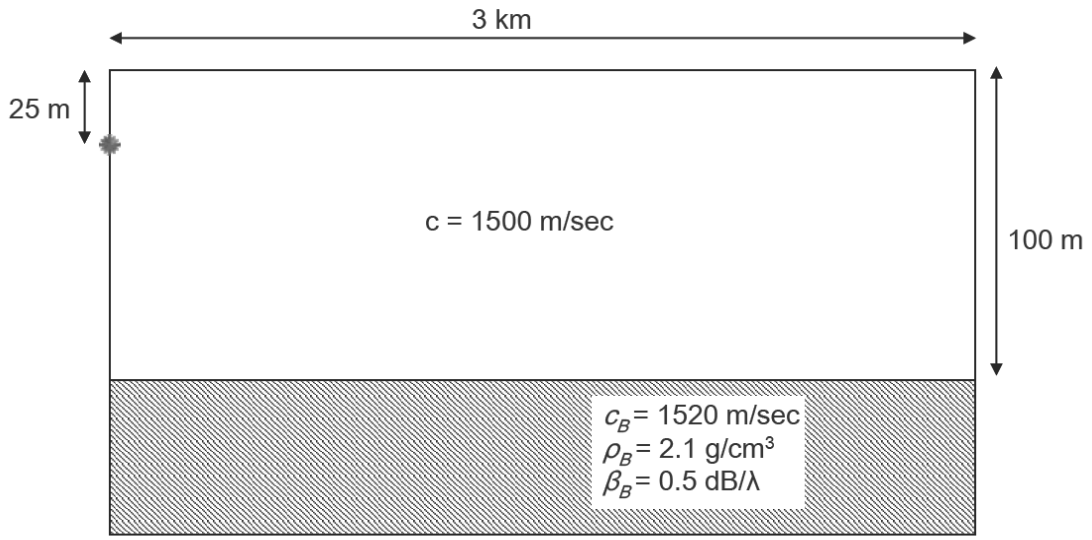


Figure 4.1: Environment of Test Case I.

Projection cost function also fails to drive us to a minimum.

Since the objective is to recover the true bottom layer with experimental data, we expose the results obtained by the two of three cost functions defined in section 3.4: Amplitude Projection and Normalized $L_1$. These cost functions are phase-free since they are making use of the amplitude of the field, only.

### 4.1.1 Test Case I

In this test case we consider an oceanic environment as shown in Fig. 4.1.

The initial values introduced into the scheme are $\rho_0 = 3.0$, $c_0 = 1580.0$ m/sec and $\beta_0 = 0.0$ dB/$\lambda$. The true values are $\rho_B = 2.1$, $c_B = 1520.0$ m/sec and $\beta_B = 0.5$ dB/$\lambda$, where the subscript $_B$ denotes the bottom. Inversions were performed for a frequency of 50 Hz with 13 receivers and for 200 Hz with 25 receivers. The equidistant receivers are placed at a range of 3 km.

| Frequency source (Hz) | No. of Iterations | Calculated value of $\rho$ | Calculated value of $c$ | Calculated value of $\beta$ | Time (sec) |
|---|---|---|---|---|---|
| 50 | 11611 | 2.15954566 | 1518.78112793 | 0.41337642 | 582 |
| 200 | 6695 | 2.10009289 | 1520.00073242 | 0.50000596 | 445 |

Table 4.1: Observed values from the IFD code. Amplitude Projection cost function.

| Frequency source (Hz) | No. of Iterations | Calculated value of $\rho$ | Calculated value of $c$ | Calculated value of $\beta$ | Time (sec) |
|---|---|---|---|---|---|
| 50 | 15066 | 2.11150312 | 1521.53698730 | 0.58567387 | 755 |
| 200 | 14365 | 2.10027885 | 1520.00756836 | 0.49979678 | 952 |

Table 4.2: Observed values from the IFD code. Normalized $L_1$ cost function.

In Tables 4.1 and 4.2 the observed values at the receiver array were obtained by solving Eq. (2.26) using the IFD+Impedance code. The multipliers used are $\alpha_\rho = 1$, $\alpha_c = 5000$ and $\alpha_\beta = 1$, for 50 Hz with both two cost functions. For 200 Hz we used $\alpha_\rho = 1$, $\alpha_c = 10000$ and $\alpha_\beta = 1$ with the Amplitude Projection cost function whereas $\alpha_\rho = 1$, $\alpha_c = 5000$ and $\alpha_\beta = 1$ for the Normalized $L_1$ cost function.

In Tables 4.3 and 4.4 the observed values at the receiver array were obtained from a Normal Mode (NM) code. The multipliers used for 50 Hz are $\alpha_\rho = 10$, $\alpha_c = 10000$ and $\alpha_\beta = 1$, for the Amplitude Projection cost function and $\alpha_\rho = 1$, $\alpha_c = 5000$ and $\alpha_\beta = 1$ for the Normalized $L_1$ cost function. For 200 Hz we used $\alpha_\rho = 1$, $\alpha_c = 10000$ and $\alpha_\beta = 1$ with the Amplitude Projection cost function whereas $\alpha_\rho = 1$, $\alpha_c = 5000$ and $\alpha_\beta = 1$ for the Normalized $L_1$ cost function.

In Figs. 4.2, 4.3, 4.4 and 4.5 we present the sound speed, density and attenuation plots versus the number of iterations for the two frequencies of Test Case I for both the two types of observed values.

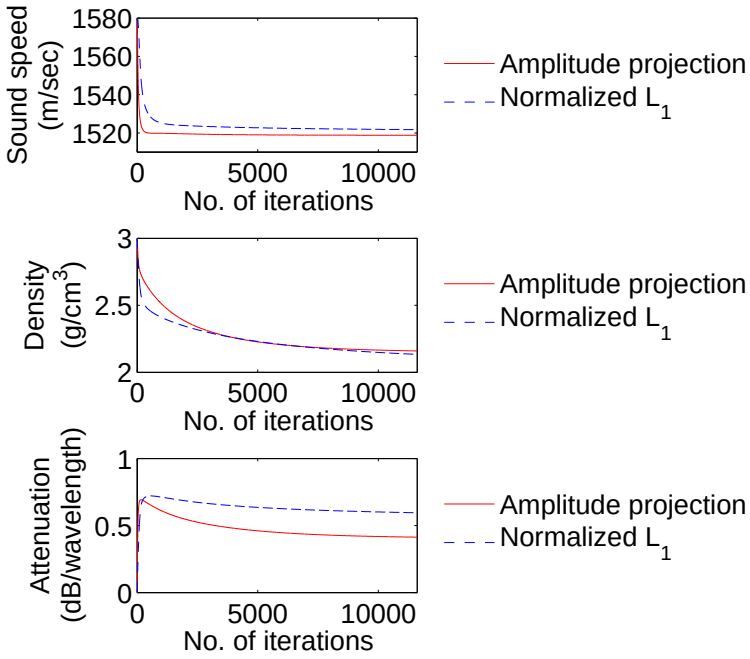


Figure 4.2: Sound speed, density and attenuation plots versus number of iterations for Test Case I with 50 Hz. Observed values from the IFD code.

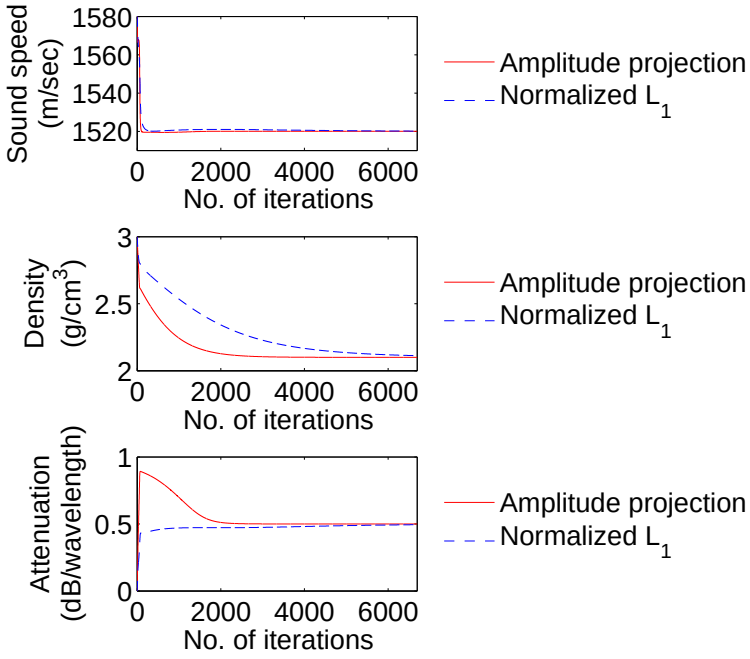


Figure 4.3: Sound speed, density and attenuation plots versus number of iterations for Test Case I with 200 Hz. Observed values from the IFD code.

| Frequency source (Hz) | No. of Iterations | Calculated value of $\rho$ | Calculated value of $c$ | Calculated value of $\beta$ | Time (sec) |
|---|---|---|---|---|---|
| 50 | 1967 | 1.99163198 | 1524.10607910 | 0.49045381 | 98 |
| 200 | 13123 | 2.05241036 | 1518.40014648 | 0.42595682 | 874 |

Table 4.3: Observed values from a NM code. Amplitude Projection cost function.

| Frequency source (Hz) | No. of Iterations | Calculated value of $\rho$ | Calculated value of $c$ | Calculated value of $\beta$ | Time (sec) |
|---|---|---|---|---|---|
| 50 | 10795 | 2.17805433 | 1521.24389648 | 0.35005012 | 540 |
| 200 | 12177 | 1.93570197 | 1518.36547852 | 0.47537878 | 808 |

Table 4.4: Observed values from a NM code. Normalized $L_1$ cost function.

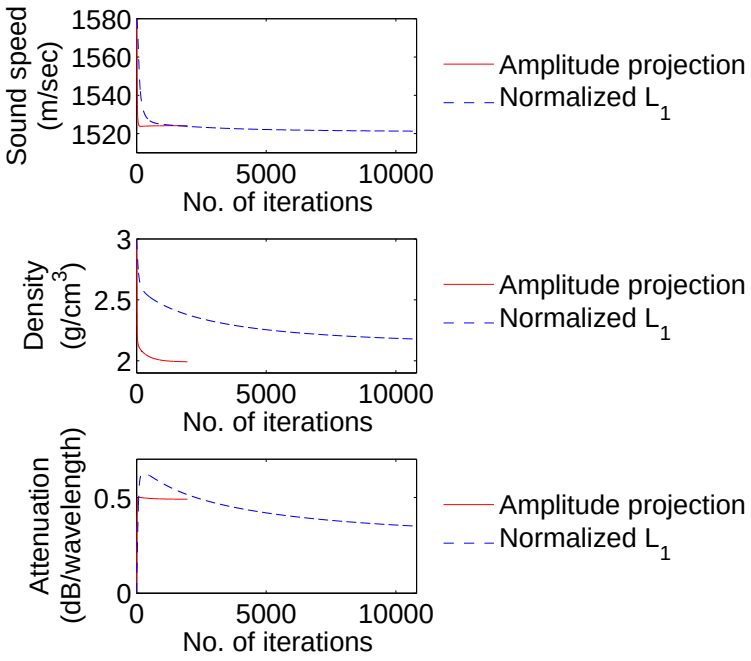


Figure 4.4: Sound speed, density and attenuation plots versus number of iterations for Test Case I with 50 Hz. Observed values from a NM code.

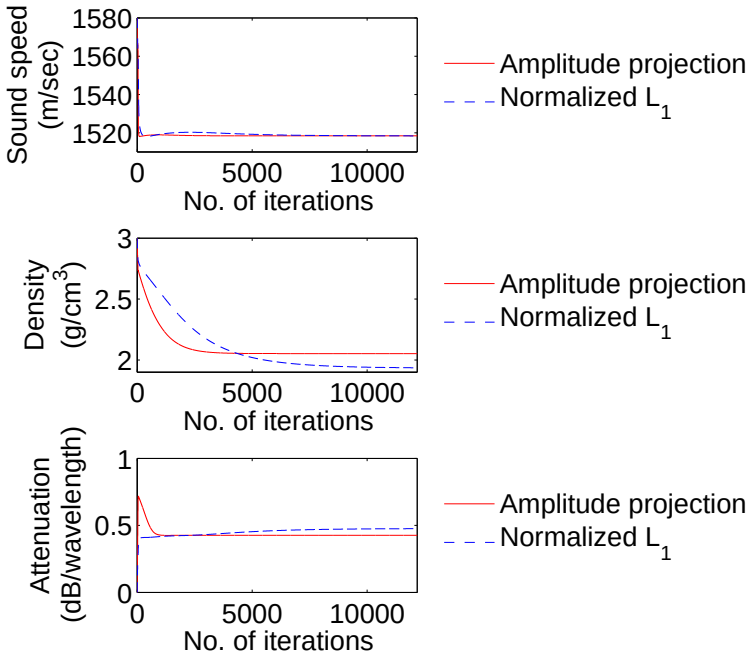


Figure 4.5: Sound speed, density and attenuation plots versus number of iterations for Test Case I with 200 Hz. Observed values from a NM code.

### 4.1.2 Test Case II

This test case was proposed by M. Meyer and J.P. Hermand [29]. It consists of a realistic sea environment of South Elba and is based on acoustic parameters obtained by full-field inversions for the YELLOW SHARK 94 experiments in the area south of the island of Elba, Italy, during an oceanographic survey with a towed-oscillating CTD profiler [28].

The waveguide consists of a water column with an average depth of 113.1 m, where the density is 1.03 g/cm$^3$. The range average of the sound speed profiles, measured during one of the experimental runs, is strongly downward refracting as shown in Fig. 4.6. A sediment layer of clay with thickness 7.5 m follows, with density $\rho_s$=1.5 g/cm$^3$ and attenuation $\beta_s$ = 0.03 dB/$\lambda$. At the top of the sediment layer the sound speed is 1470 m/sec whereas at the bottom is 1485 m/sec. The homogeneous fluid half-space, which extends below 120.6 m,

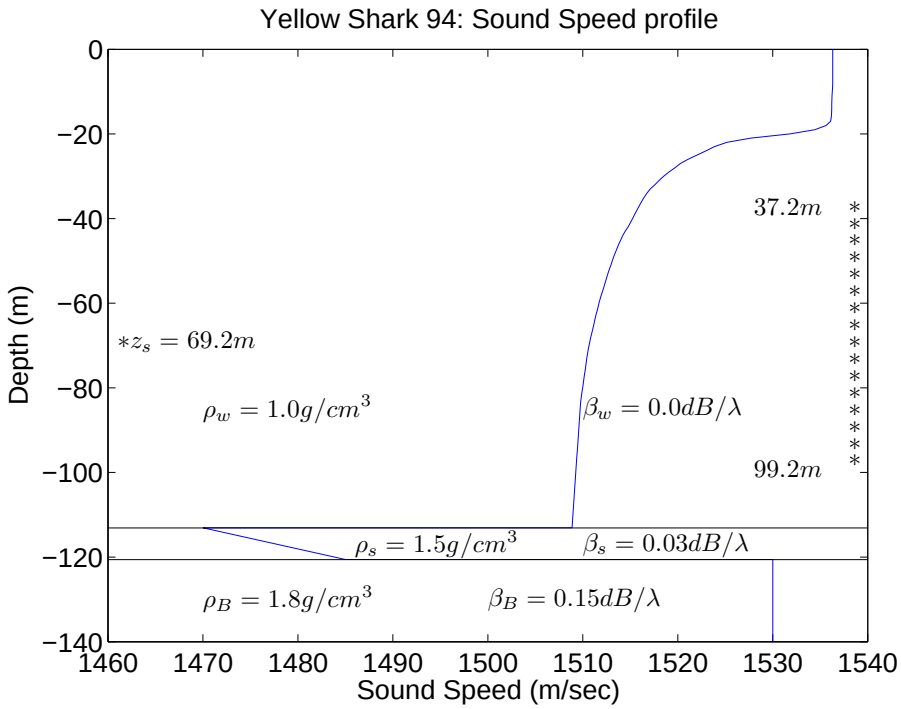


Figure 4.6: Physical properties of the sea environment of Test Case II (based on YELLOW SHARK'94 experiment simulation of the South Elba physical environment[28]).

consists of silty clay with sound speed 1530 m/sec, density $\rho_B$ =1.8 g/cm$^3$ and attenuation $\beta_B$ = 0.15 dB/$\lambda$. The source was located in a depth of 69.2 m. 32 equidistant hydrophones were placed from 37.2 m to 99.2 m in depth, at a range of 9.026 km. A set of 6 frequencies was used: 250 Hz, 315 Hz, 400 Hz, 500 Hz, 630 Hz, 800 Hz.

In Table 4.5 and 4.6 the observed values at the receiver array were obtained by solving Eq. (2.26) using the IFD+Impedance code. The values of the multipliers for 250, 315, 400 and 630 Hz are $\alpha_\rho = 10$, $\alpha_c = 10000$ and $\alpha_\beta = 0.1$, for both cost functions, whereas for 500 and 800 Hz we used $\alpha_\rho = 100$, $\alpha_c = 10000$ and $\alpha_\beta = 1$.

In Table 4.7 and 4.8 the observed values at the receiver array were obtained

| Frequency source (Hz) | No. of Iterations | Calculated value of $\rho$ | Calculated value of $c$ | Calculated value of $\beta$ | Time (sec) |
|---|---|---|---|---|---|
| 250 | 2051 | 1.79984426 | 1529.99841309 | 0.14983325 | 811 |
| 315 | 8966 | 1.80174923 | 1530.01098633 | 0.15071066 | 3550 |
| 400 | 1096 | 1.81675851 | 1531.06774902 | 0.15896057 | 1468 |
| 500 | 1751 | 1.80031848 | 1529.99914551 | 0.14997886 | 2360 |
| 630 | 1081 | 1.80047941 | 1529.99731445 | 0.15004224 | 1500 |
| 800 | 1507 | 1.80424428 | 1530.00988770 | 0.15015587 | 2064 |

Table 4.5: Observed values from the IFD code. Amplitude Projection cost function.

from a NM code. The values of the multipliers for 250 and 315 Hz were $\alpha_\rho = 10$, $\alpha_c = 10000$ and $\alpha_\beta = 0.1$ for the Amplitude Projection cost function, whereas for the Normalized $L_1$ cost function we used $\alpha_\rho = 10$, $\alpha_c = 5000$ and $\alpha_\beta = 0.1$. For 400 Hz we used $\alpha_\rho = 2$, $\alpha_c = 10000$ and $\alpha_\beta = 1$, for both cost functions.

In Table 4.9 and 4.10 the observed values at the receiver array were obtained from Experimental data. The values of the multipliers for 400 Hz were $\alpha_\rho = 10$, $\alpha_c = 5000$ and $\alpha_\beta = 0.1$, for both cost functions. For 630 Hz we used $\alpha_\rho = 10$, $\alpha_c = 10000$ and $\alpha_\beta = 1$ for the Amplitude Projection cost function, whereas for the Normalized $L_1$ cost function we used $\alpha_\rho = 10$, $\alpha_c = 5000$ and $\alpha_\beta = 0.1$. The multipliers for the multi-frequency case are $\alpha_\rho = 1$, $\alpha_c = 5000$ and $\alpha_\beta = 0.01$

The initial values were $\rho_0 = 3.0$, $c_0 = 1580$ m/sec and $\beta_0 = 0$ dB/$\lambda$ for all cases except for 315 Hz with observed values from a NM code where we started from $\rho_0 = 3.0$, $c_0 = 1550$ m/sec and $\beta_0 = 0$ dB/$\lambda$.

| Frequency source (Hz) | No. of Iterations | Calculated value of $\rho$ | Calculated value of $c$ | Calculated value of $\beta$ | Time (sec) |
|---|---|---|---|---|---|
| 250 | 2271 | 1.79993451 | 1529.99914551 | 0.14989185 | 899 |
| 315 | 11146 | 1.80078423 | 1530.00463867 | 0.15030560 | 4421 |
| 400 | 2130 | 1.82643867 | 1530.84667969 | 0.16291974 | 2865 |
| 500 | 1511 | 1.80033088 | 1529.99926758 | 0.14998716 | 2033 |
| 630 | 484 | 1.80074108 | 1529.99768066 | 0.15053464 | 653 |
| 800 | 687 | 1.80424452 | 1530.00988770 | 0.15015595 | 928 |

Table 4.6: Observed values from the IFD code. Normalized $L_1$ cost function.

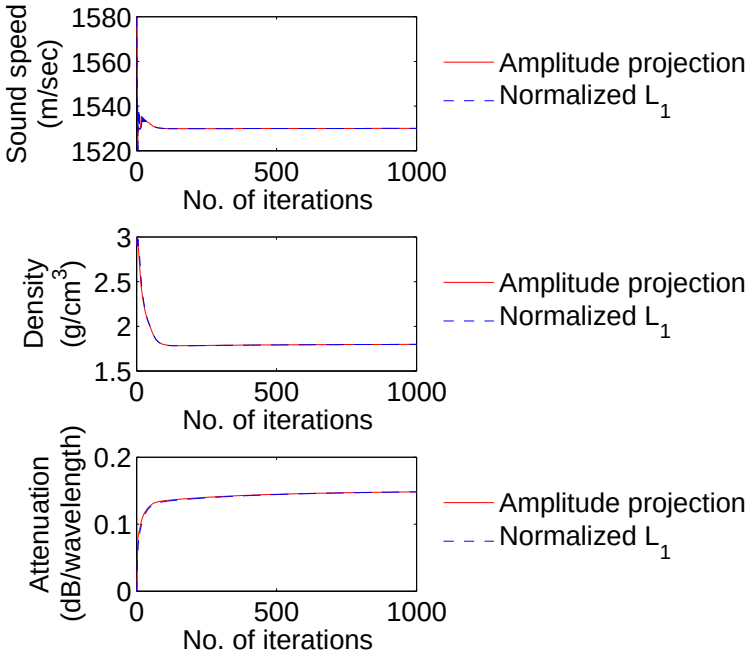


Figure 4.7: Sound speed, density and attenuation plots versus number of iterations for Test Case II with 250 Hz. Observed values from the IFD code.

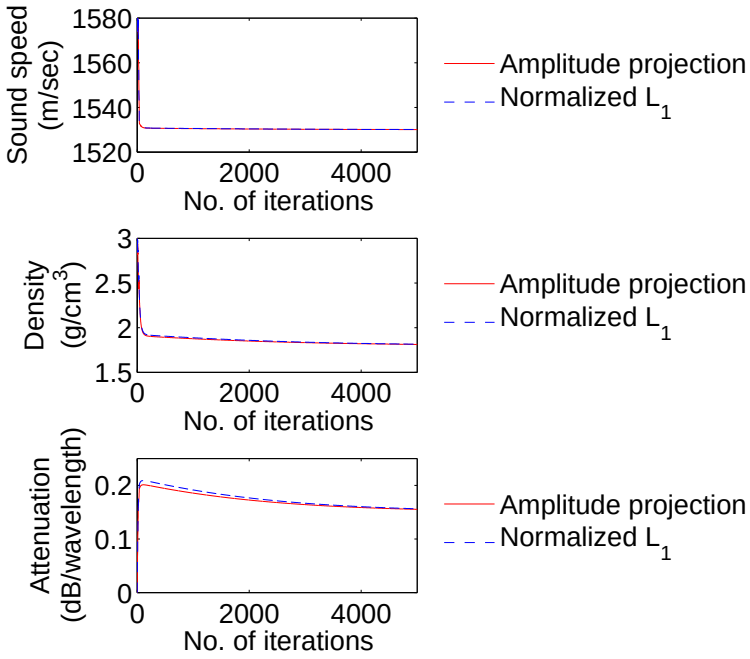


Figure 4.8: Sound speed, density and attenuation plots versus number of iterations for Test Case II with 315 Hz. Observed values from the IFD code.

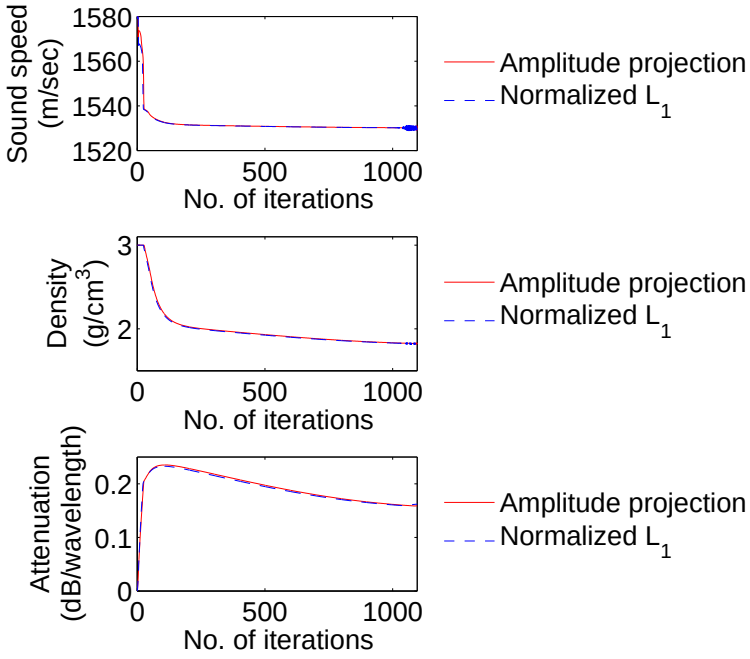


Figure 4.9: Sound speed, density and attenuation plots versus number of iterations for Test Case II with 400 Hz. Observed values from the IFD code.

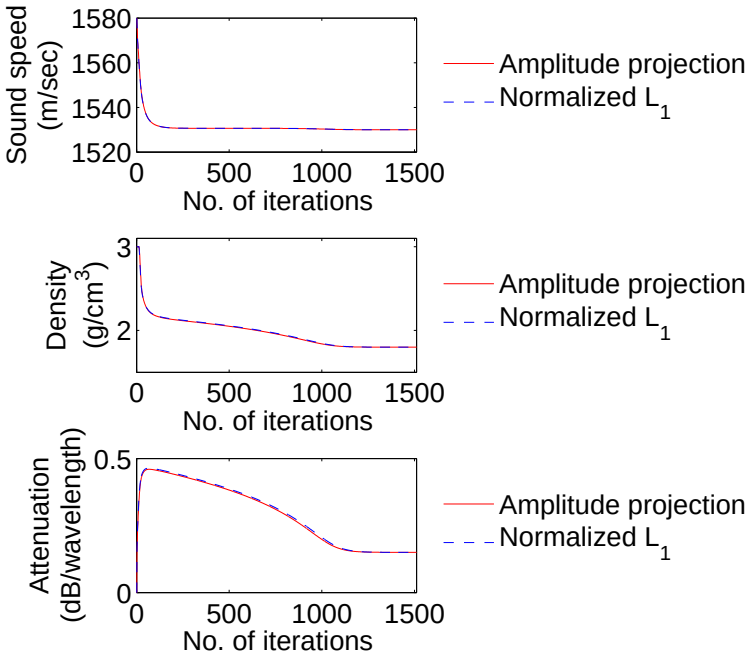


Figure 4.10: Sound speed, density and attenuation plots versus number of iterations for Test Case II with 500 Hz. Observed values from the IFD code.

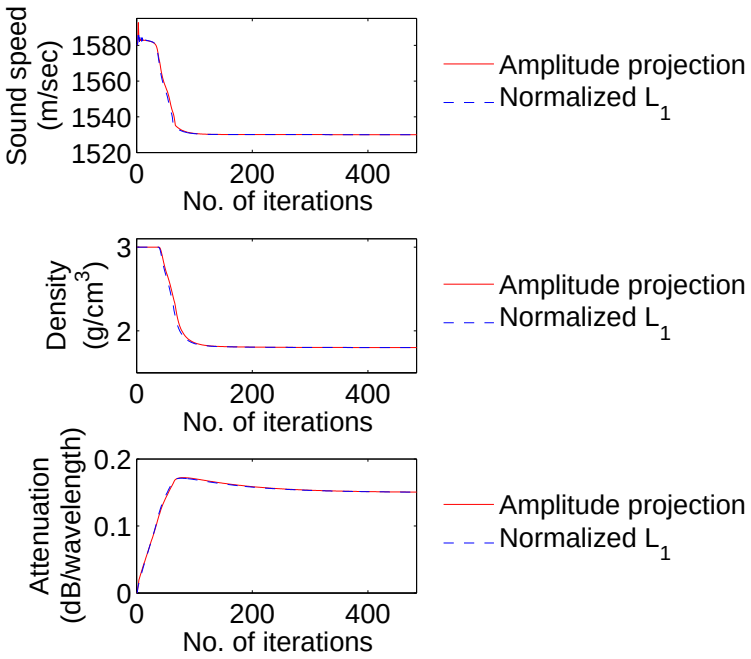


Figure 4.11: Sound speed, density and attenuation plots versus number of iterations for Test Case II with 630 Hz. Observed values from the IFD code.

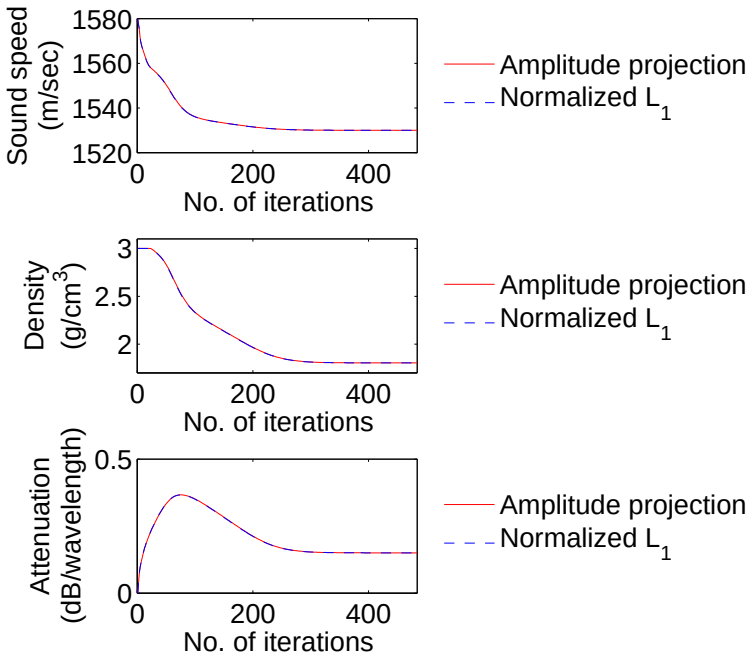


Figure 4.12: Sound speed, density and attenuation plots versus number of iterations for Test Case II with 800 Hz. Observed values from the IFD code.

| Frequency source (Hz) | No. of Iterations | Calculated value of $\rho$ | Calculated value of $c$ | Calculated value of $\beta$ | Time (sec) |
|---|---|---|---|---|---|
| 250 | 2755 | 2.14878678 | 1528.29980469 | 0.14391637 | 1098 |
| 315 | 3035 | 1.80213368 | 1527.00390625 | 0.13148127 | 1208 |
| 400 | 1131 | 1.99025083 | 1526.93518066 | 0.13116714 | 1520 |

Table 4.7: Observed values from a NM code. Amplitude Projection cost function.

| Frequency source (Hz) | No. of Iterations | Calculated value of $\rho$ | Calculated value of $c$ | Calculated value of $\beta$ | Time (sec) |
|---|---|---|---|---|---|
| 250 | 2132 | 2.14881325 | 1528.29968262 | 0.14397869 | 844 |
| 315 | 2786 | 1.79441345 | 1527.35888672 | 0.12889819 | 1103 |
| 400 | 1141 | 1.99037361 | 1526.93298340 | 0.13120359 | 1527 |

Table 4.8: Observed values from a NM code. Normalized $L_1$ cost function.

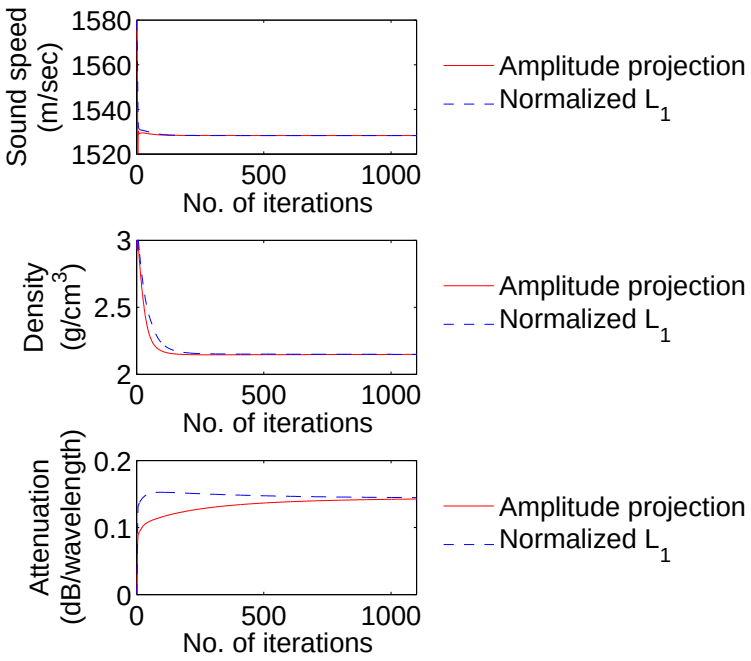


Figure 4.13: Sound speed, density and attenuation plots versus number of iterations for Test Case II with 250 Hz. Observed values from a NM code.

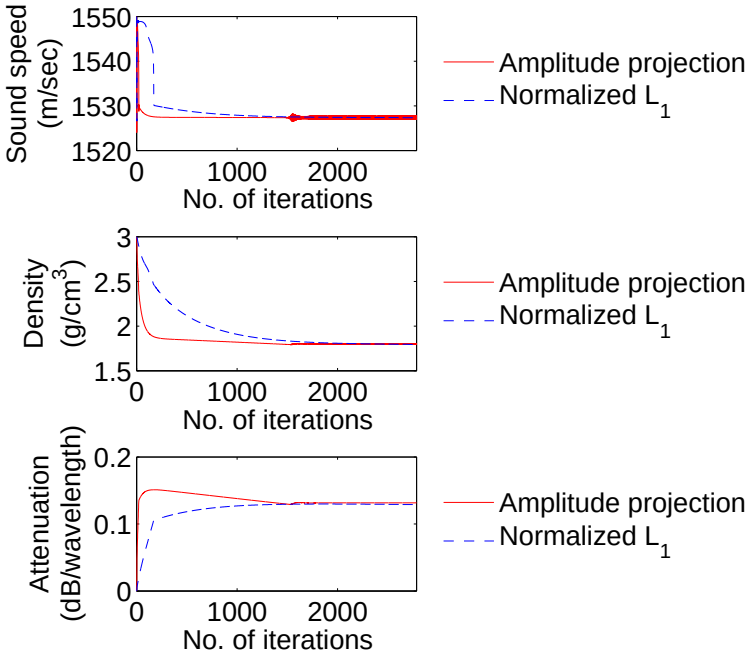


Figure 4.14: Sound speed, density and attenuation plots versus number of iterations for Test Case II with 315 Hz. Observed values from a NM code.

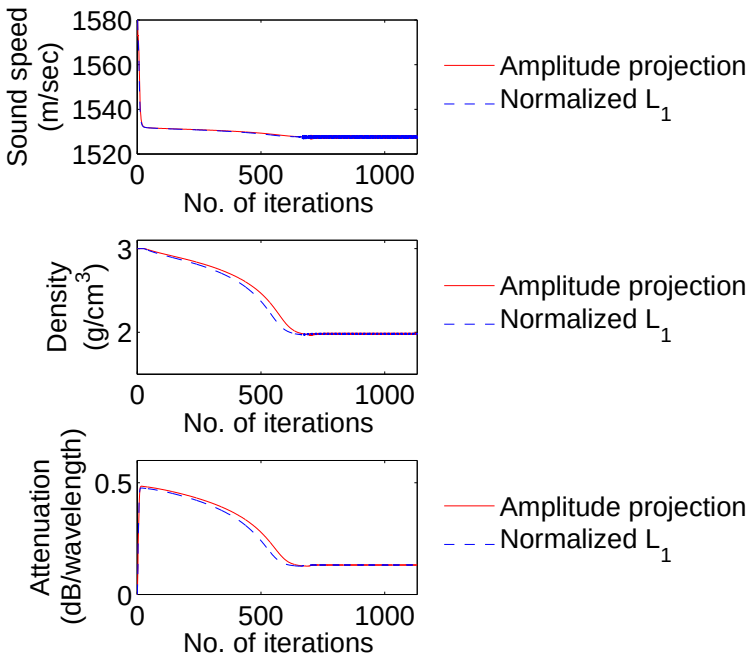


Figure 4.15: Sound speed, density and attenuation plots versus number of iterations for Test Case II with 400 Hz. Observed values from a NM code.

| Frequency source (Hz) | No. of Iterations | Calculated value of $\rho$ | Calculated value of $c$ | Calculated value of $\beta$ | Time (sec) |
|---|---|---|---|---|---|
| 400 | 1656 | 1.72317553 | 1530.02673340 | 0.11196246 | 2213 |
| 630 | 1204 | 1.62510777 | 1527.88000488 | 0.25140700 | 1609 |
| 400+630 | 4838 | 1.62853754 | 1528.26647949 | 0.23438135 | 12971 |

Table 4.9: Observed values from Experimental data. Amplitude Projection cost function.

| Frequency source (Hz) | No. of Iterations | Calculated value of $\rho$ | Calculated value of $c$ | Calculated value of $\beta$ | Time (sec) |
|---|---|---|---|---|---|
| 400 | 1142 | 1.72451305 | 1529.96606445 | 0.11196236 | 1526 |
| 630 | 1155 | 1.64396119 | 1528.29260254 | 0.25233480 | 1544 |
| 400+630 | 1638 | 1.60066521 | 1528.22827148 | 0.20962268 | 4408 |

Table 4.10: Observed values from Experimental data. Normalized $L_1$ cost function.

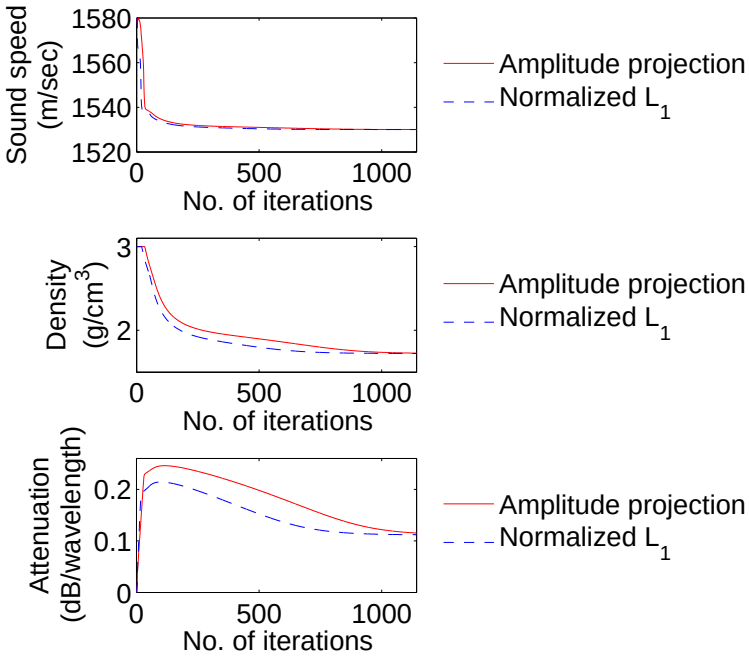


Figure 4.16: Sound speed, density and attenuation plots versus number of iterations for Test Case II with 400 Hz. Observed values from Experimental data.

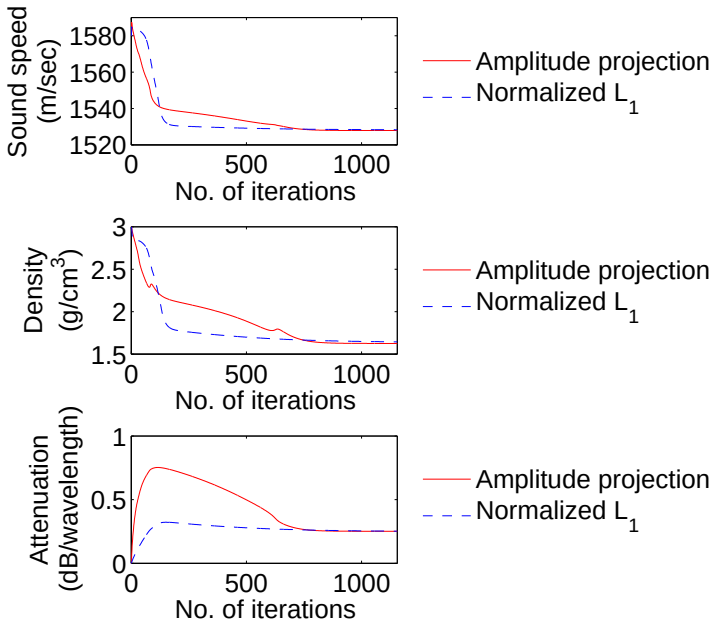


Figure 4.17: Sound speed, density and attenuation plots versus number of iterations for Test Case II with 630 Hz. Observed values from Experimental data.

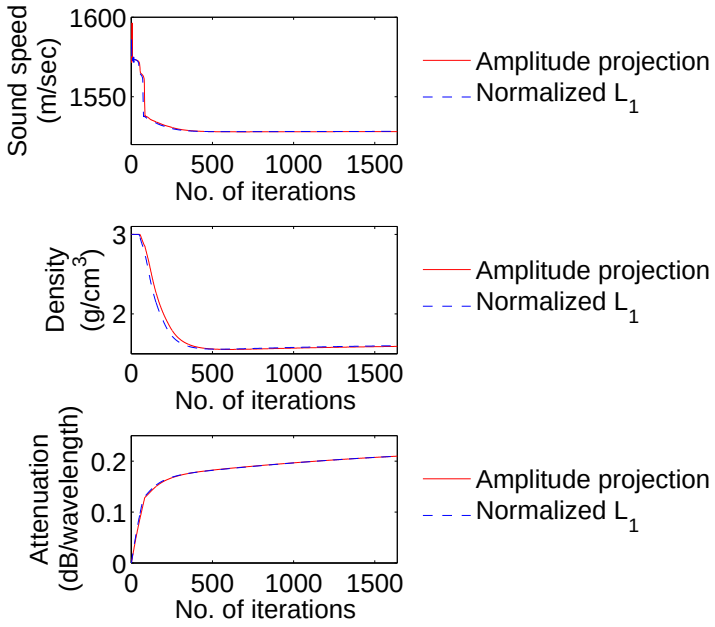


Figure 4.18: Sound speed, density and attenuation plots versus number of iterations for Test Case II with 400+630 Hz. Observed values from Experimental data.

## 4.2 Discussion

The first observation is that for observed values from the IFD+Impedance code the iterative scheme converges to the true zero minimum of both the cost functions, since the complex pressure at the receiver array is simulated by the direct model used in the inversion with the correct values of density, sound speed and attenuation of the bottom. We must note that for the Test Case I with 50 Hz there is an error in the recovered values of the parameters. This is justified by the fact that for this frequency where the wavelength is large relative to the depth of the water, the interaction of the wave with the bottom boundary is small, so the information coming from the boundary condition is not sufficient for the inversion. Results are accurate for Test Case I with 200 Hz, as well as for Test Case II with all frequencies.

When the observed values are obtained by a Normal Mode code, the iteration still converges to the true minimum of both the cost functions with a reasonable, small error in the recovered values, for Test Case I with the two frequencies and Test Case II with 250 Hz, 315 Hz and 400 Hz.

In Figure 4.19 we can see the normalized magnitude square

$$nms(i) = \frac{|u^i_{obs}|^2}{\sum_{i=1}^{32} |u^i_{obs}|^2}$$

of the measured field, the field obtained by the IFD+Impedance code (with $z_2$ at 120.5 m) [1] and by a Normal Mode code, at 9.026 km, from 37.2 to 99.2 m, for the environment in Figure 4.6.

It is obvious from the definition of the two cost functions we have used (Amplitude Projection, Normalized $L_1$) that comparing the normalized magnitude square (nms) of the field from the IFD+Impedance code with the nms of the

[1] The true bottom of the sediment layer as it has been measured during the experiment is at 120.6 m in depth.

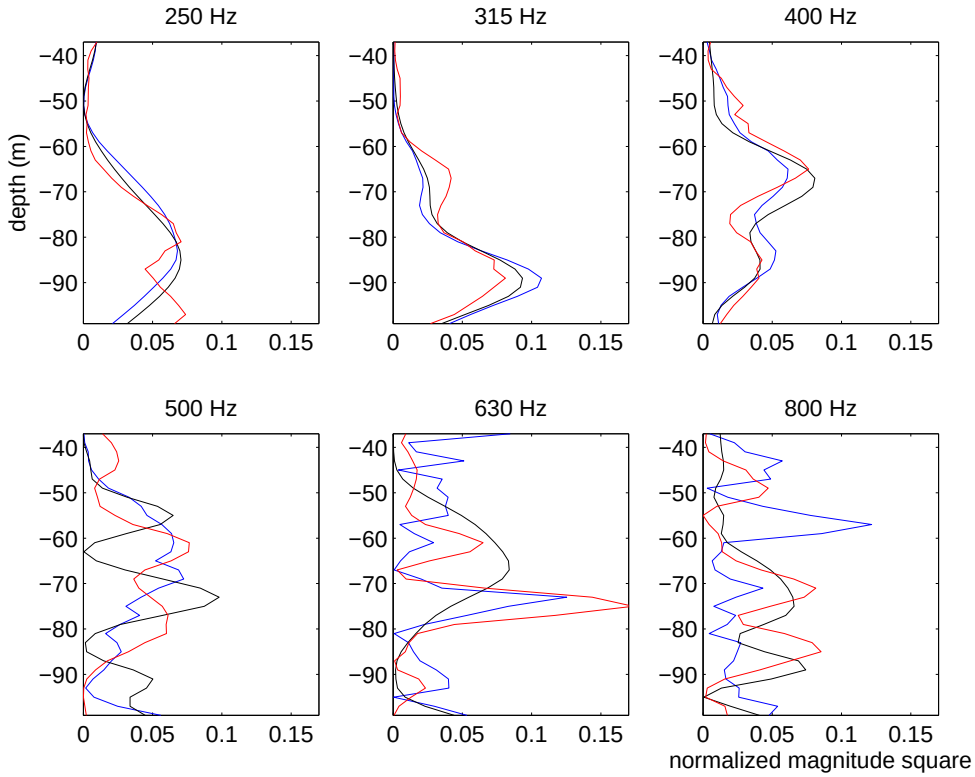


Figure 4.19: Normalized Magnitude Square of modelled fields: IFD+Impedance with $z_2 = 120.5$ m (blue line), Normal Mode (black line) and measured fields (red line) for the sea environment of Test Case II at 9 km.

field from a NM code or the measured field, we can have a first estimation for the convergence with data from a NM code or the experimental data.

For example, we observe that for the frequencies of 500, 630 and 800 Hz, the $nms$ of the Normal Mode data does not fit at all with the $nms$ of the IFD+Impedance data. Therefor, we have no hope for convergence for these frequencies.

When the observed values are obtained by Experimental data, we have convergence to the true minimum of both the cost functions only for 400 and 630 Hz, with $z_2$ at 120.5 m. This fact can also be justified by observing the blue and red lines in Figure 4.19.

The rate of convergence depends on the choice of the multiplier $\alpha = (\alpha_\rho, \alpha_c, \alpha_\beta)$. The need of multiplier arises from the different scale of variation of density, sound speed and attenuation.

The method presented, in this work, is also applicable for the case of horizontal array measurements.

## 4.3 Conclusions

The NtD map of the form of a convolution integral, is proven an efficient tool in evaluating the gradient of the cost function in an optimal control formulation of the inversion leading to the recovering of the true bottom with experimental data.

In general, the convergence of the iteration scheme of an optimization problem depends on the proximity of the initial guess to the optimal values of the controls. It is worth noticing that the proposed scheme converges to the correct bottom parameters with initial density, sound speed and attenuation in a rather large

neighborhood of $(\rho_B, c_B, \beta_B)$.

We must also point out that both phase-independent cost functions give convergent schemes.

It is believed that a better approximation to the square-root operator of GPE as well as the calculation of the derivative of the kernel $G(p_1, p_2, p_3, r, z_c)$ in the NtD map with respect to $p_1, p_2$ and $p_3$ for the WAPE, will give better results.

Application of the Optimal Control Adjoint Method for recovering the properties of the semi-infinite lower layer $D_{L+1}$ as well as these of the layer $D_L$ above, is a challenge. For this inverse problem we have 7 control parameters, i.e. two densities, two sound speeds, two attenuation coefficients and the thickness of the layer $D_L$.

# Bibliography


[1] F. D. Tappert, "The parabolic approximation method", in *Wave Propagation and Underwater Acoustics*, J. B. Keller and J. S. Papadakis (Eds.), *Lecture Notes in Physics*, Vol. 70, (Springer-Verlag, Heidelberg, 1977), pp. 224–287.

[2] Mireille Levy, *Parabolic equation methods for electromagnetic wave propagation* (The Institution of Electrical Engineers, London, 2000).

[3] D. Lee, A. D. Pierce, and E. C. Shang, "Parabolic equation development in the twentieth century", *J. Comput. Acoust.* **8**(4), 527–637 (2000).

[4] J. A. Davis, D. White, and R. C. Cavanagh, "NORDA parabolic equation workshop", Rep. TN-143, Naval Ocean Research and Development Activity, Stennis Space Center, MS (1982)

[5] F. B. Jensen, W. A. Kuperman, M. B. Porter and H. Schmidt, *Computational Ocean Acoustics* (American Institute of Physics, New York, 1994).

[6] R. R. Greene, "The rational approximation to the acoustic wave equation with bottom interaction" *J. Acoust. Soc. Am.* **76**, 1764–1773 (1984).

[7] J. S. Papadakis, "Impedance Formulation of the Bottom Boundary Condition for the Parabolic Equation Model in Underwater Acoustics," *NORDA*

*Parabolic Equation Woskshop I*, editors J. A. Davis, D. White and R.C. Cavanagh, 31 March – 3 April 1981, Tech, Note 143, Naval Ocean Research and Development Activity, NSTL Station, MS. 1982, available from NTIS, No AD-121 932 (1981) p. 83.

[8] J. S. Papadakis,"Impedance bottom boundary conditions for parabolic-type approximations in Underwater Acoustics", *Procceedings of the Second Parabolic Equation Workshop*, 1991, NRL, pp. 265–270.

[9] J. S. Papadakis, "Exact, nonreflecting boundary conditions for parabolic-type approximations in underwater acoustics," *J. Comput. Acoust.* **2**, 83–98 (1994).

[10] J. S. Papadakis, M. I. Taroudakis, P. J. Papadakis, and B. Mayfield, "A new method for a Realistic Treatment of the Sea Bottom in the Parabolic Approximation," *J. Acoust. Soc. Am.* **92**, 2030–2038 (1992).

[11] J. S. Papadakis and B. Pelloni, "A method for the treatment of a sloping sea bottom in the parabolic approximation" *J. Comput. Acoust.* **4**(1), 89–100 (1996).

[12] S. W. Marcus, "A generalized impedance method for application of the parabolic approximation to underwater acoustics", *J. Acoust. Soc. Am.* **90**, 391–398 (1991).

[13] A. Arnold and M. Ehrhardt, "Discrete transparent boundary conditions for wide angle parabolic equations in underwater acoustics", *J. Comput. Phys.* **145**(2). 611–638 (1998).

[14] D. Yevick and D. J. Thomson, "Nonlocal boundary conditions for finite difference parabolic equation solvers," *J. Acoust. Soc. Am.* **106**, 143–150 (1999).

[15] D. Yevick and D. J. Thomson, "Impedance-matched absorbers for finite difference parabolic equation algorithms," *J. Acoust. Soc. Am.* **107**, 1226–1234 (2000).

[16] D. Mikhin, "Exact discrete nonlocal boundary conditions for high-order Padé parabolic equations," *J. Acoust. Soc. Am.* **116**, 2864–2875 (2004).

[17] G. A. Cambell and R. M. Foster, *Fourier Integrals for Practical Applications*, (Van Nostrand, New York, 1951), p.53.

[18] D. Lee and G. Botseas, "An implicit finite-difference computer model for solving the parabolic equation", NUSC Tech. Report 6659 (1982).

[19] J. S. Papadakis and B. Mayfield, "IFD+IMPEDANCE Impedance boundary conditions along the bottom interface incorporated in the implicit finite-difference code for solving the parabolic equation", IACM Report (1986).

[20] P. R. McGillivray, D. W. Oldenburg, "Methods for Calculating Fréchet Derivatives and Sensitivities for the Non-linear Inverse Problem: a Comparative-Study", *Geophys. Prospect* **38**, 499–524 (1990).

[21] Y. Jarny, M.N. Ozisik, J.P. Bardon, "A general optimization method using adjoint equation for solving multidimensional inverse heat conduction", *International Journal of Heat and Mass Transfer* **34**, 2911-2919 (1991).

[22] T. Wang, M. Oristaglio, A. Tripp, and G. Hohmann, "Inversion of diffusive transient electromagnetic data by a conjugate-gradient method, *Radio Sci.* **29**, 1143–1156 (1994).

[23] S. J. Norton, "Theory of eddy current inversion", *J. Appl. Phys.* **73**, 501–512 (1993).

[24] S. J. Norton, "A general nonlinear inverse transport algorithm using forward and adjoint flux computations", IEEE Transactions on Nuclear Science, **44**, issue 2, pp. 153-162 (1997).

[25] S. J. Norton, "Iterative inverse scattering algorithms: Methods of computing the Fréchet derivatives", *J. Acoust. Soc. Am.* **106**, 2653–2660 (1999).

[26] J. S. Papadakis and E.T. Flouri, "Geoacoustic Optimal Control Adjoint Inversion for a Parabolic Equation with a Neumann to Dirichlet Map Bottom Boundary Condition", submitted to *Acta Acustica united with ACUSTICA*, 2007.

[27] J. S. Papadakis and E.T. Flouri, "Geoacoustic Adjoint-based Inversion for a Parabolic Equation with a Neumann to Dirichlet Map Bottom Boundary Condition", *Procceedings of the* $2^{nd}$ *Interntional Conference on Underwater Acoustic Measurements: Technologies Results*, Heraklion, Crete, 25–29 June, 2007.

[28] J.-P. Hermand, "Broad-band geoacoustic inversion in shallow water from waveguide impulse response measurements on a single hydrophone: theory and experimental results", *IEEE J. Ocean. Eng.* **24**(1), 41–66 (1999).

[29] M. Meyer and J.-P. Hermand, "Toward an Adjoint-based Inversion of broad-band acoustic measurements in a shallow water environment", Proceedings of the *Int. Conference on Underwater Acoustic Measurements: Technologies & Results*, Heraklion, Crete, Greece, 28th June – 1st July 2005.